PHYSICAL REVIEW C VOLUME 19, NUMBER 1 JANUARY 1979

States in ^{106}Cd populated by heavy-ion (xn) reactions interpreted by a two-quasiparticle-plus-rotor model

L. E. Samuelson,* J. A. Grau,† S. I. Popik, F. A. Rickey, and P. C. Simms
Tandem Accelerator Laboratory, Purdue University, West Lafayette, Indiana 47907
(Received 20 July 1978)

Levels in ^{106}Cd were studied using (heavy-ion, $xn\gamma$) reactions. The experiments included γ-ray yields as a function of bombarding energy, γ-ray angular distributions, γ-ray linear polarizations, and γ-γ coincidence measurements. The decay scheme, which includes 85 γ-ray transitions, is similar to those reported for ^{108}Cd and ^{102,104,106}Pd. In addition to the ground-state band, there appear two negative-parity collective bands built on two quasineutron states. The yrast positive-parity states appear dominated by intruder states at 8^+, 3044.23 keV (two-quasiproton), 10^+, 4435.08 keV (two-quasineutron), and 12^+, 4659.81 keV (four-quasiparticle). The results are compared to calculations from a two-quasiparticle plus slightly deformed rotor model which utilizes a variable moment of inertia.

[NUCLEAR STRUCTURE ^{96}Mo(^{13}C, $3n\gamma$) at 45 MeV; ^{97}Mo(^{12}C, $3n\gamma$) at 45 MeV, ^{94}Zr(^{16}O, $4n\gamma$) at 63 MeV: measured $I_\gamma(E(^{13}\text{C}))$, $I_\gamma(E(^{16}\text{O}))$, $I_\gamma(\theta)$ ^{13}C, ^{16}O, P_γ[^{16}O], γ-γ coin [^{12}C, ^{16}O], γ-γ DCO[^{12}C]. ^{106}Cd deduced levels, J, π, γ multipolarity. Rotational model calculations. Enriched targets, Ge(Li) detectors.]

I. INTRODUCTION

The study of transitional nuclei represents an intriguing challenge to the field of nuclear structure. Microscopic calculations, such as those based on the shell model, become extremely complicated whenever there are more than a few particles outside of closed shells. Thus it is useful to identify collective modes of excitation that can be used to interpret nuclear phenomena. There is extra appeal if concepts that have proven valuable in one region can be applied to a broader range of nuclei.

Nuclei in the mass-100 region ($Z < 50, N > 50$) provide an excellent opportunity to test the hypothesis that rotational phenomena play an important role in transitional nuclei. Recent investigations[1,2] have shown that the states observed following (HI, $xn\gamma$) reactions in ^{101,103,105}Pd and ^{105,107,109}Cd are in good agreement with a Coriolis coupling calculation using a slightly deformed, symmetric rotor with variable moment of inertia. The Coriolis calculation used for Pd and Cd nuclei is the same as that used for strongly deformed nuclei,[3] except that the deformation is smaller and a variable moment of inertia is included. The need for a variable moment of inertia is strongly implied by the systematics of energy levels in the ground-state bands of even-even nuclei in this region. A variable moment of inertia does not necessarily represent a departure from the situation observed for strongly deformed nuclei. When the nuclear deformation is small, a larger frequency of rotation must be associated with a given angular momentum. If a change in the moment of inertia is caused by Coriolis antipairing or centrifugal stretching, the effect would be large when the angular frequency is large. From this point of view, a relatively large increase in the moment of inertia is expected as the angular momentum increases in slightly deformed nuclei. It is certainly a plausible, although not proven, idea that a change in deformation is the primary difference between mass-100 and strongly deformed nuclei.

Evidence for the interpretation of mass-100 nuclei as slightly deformed rotors has also been found in studies of the even-even nuclei ^{102,104,106}Pd (Ref. 4) and ^{108}Cd (Ref. 5). The observation that decoupled collective bands built on two-quasineutron states dominate the yrast states in these nuclei, and the appearance of a probable two-quasiproton intruder state in ^{108}Cd makes the study of ^{106}Cd interesting. Accordingly, we have studied the ^{106}Cd nucleus using several (heavy-ion, $xn\gamma$) reactions.

Until recently very little was known about the high-spin states of ^{106}Cd. Daniere *et al.*,[6] using the ^{104}Pd ($\alpha, 2n\gamma$) ^{106}Cd reaction, have presented a level scheme of ^{106}Cd up to 4659.8 keV in excitation and spins up to 12. In the present paper, a detailed analysis of the (heavy-ion, $xn\gamma$) experiments leading to the ^{106}Cd nucleus is presented and the level

scheme of Daniere *et al.*[6] is greatly extended with many spin and parity assignments having been made firm. An interpretation based upon a two-quasiparticle plus slightly deformed rotor model will be shown to describe well the features of ^{106}Cd. It will be seen that two-quasiproton states strongly influence the yrast states of ^{106}Cd, and that a new four-quasiparticle band has probably been found.

II. EXPERIMENTAL PROCEDURE

The experiments included excitation functions, γ-ray angular distributions, γ-ray linear polarization measurements, and γ-γ coincidence measurements following (HI, xn) reactions. Preliminary measurements on ^{106}Cd were made with the ^{94}Zr(^{16}O, $4n$)^{106}Cd reaction as a byproduct during the investigation of ^{107}Cd with the ^{94}Zr(^{16}O, $3n$)^{107}Cd reaction. Most of the data reported here was obtained with the ^{96}Mo(^{13}C, $3n$)^{106}Cd and ^{97}Mo(^{12}C, $3n$)^{106}Cd reactions where the production of ^{106}Cd is the dominant process. The ($p2n$) exit channel was the major competing process but the resulting ^{106}Ag γ rays did not interfere with many ^{106}Cd γ rays. Coulomb excitation produced more γ rays from ^{97}Mo while the yields for ^{106}Cd γ rays were comparable for the two targets, so the most useful reaction proved to be ^{96}Mo(^{13}C, $3n$)^{106}Cd.

In all experiments enriched targets (^{96}Mo 96.8% and ^{97}Mo 92.8%) in the form of rolled foils approximately 2 mg/cm^2 were used. The incident ^{12,13}C energy was 45 MeV but the average energy in the targets was about 42 MeV. Approximately 4 mg/cm^2 of Au was evaporated onto the back of the targets to stop recoiling nuclei and prevent Doppler shift in the γ-ray spectra. A 2.5×10^{-3} cm thick Au sheet was placed immediately behind the target to stop the beam. Beam currents of 10 to 20 nanoamps were supplied by the Purdue FN Tandem Van de Graaff accelerator.

The Ge(Li) detectors had active volumes of 25 to 45 cc and energy resolutions from 2.2 to 2.5 keV [full width at half maximum (FWHM) at a γ-ray energy of 1333 keV]. The energy resolution of the dual Ge(Li) detector linear polarization spectrometer was 4.5 keV.

For singles measurements a ^{60}Co source was mounted on the detector so the 1173.26- and 1332.59-keV γ rays from the source could be counted simultaneously with γ rays from the target. Since the 191.48-, 278.92-, and 547.55-keV γ rays from Coulomb excitation of the Au backing are always present, five internal reference lines of well-known energies were available in each spectrum. The nonlinearity of the detector-electronics system was measured using a ^{182}Ta and ^{152}Eu source, and γ-ray energies typically are accurate to ±50 eV.

The excitation functions were run over a range of 10 MeV to select the best incident energy for the measurements. The best energy is always on the high side of the maximum yield for γ rays from low energy states in the nucleus of interest. This choice increases competition from ($4n$), ($\alpha, 2n$), and ($p2n$) reactions but also increases the population of high angular momentum states.

Since a large number of γ rays are produced by the reaction of interest and the competing reactions, many peaks in the γ-ray singles spectrum represent more than one transition. In order to fully utilize the complex data from (HI, xn) reactions, we emphasize good statistical accuracy and precise data treatment in γ-γ coincidence measurements.[4] Three Ge(Li) detectors are used to give a threefold improvement in the coincidence data rate (typically 2000 to 4000 events per second). In this experiment more than 200 million coincidence events were recorded. 317 gates were set on γ-ray peaks and Compton backgrounds. Each gate generates three coincidence spectra, one for each pair of detectors. This obviously represents a massive data handling problem, but it is essential to obtain reliable information on important weak transitions. The data was recorded event by event on magnetic tape and sorted after the measurement to construct the coincidence spectra using a PDP-15 computer. Corrections were made for detector efficiency, fractions of peaks covered by gates, coincidence circuit efficiency, and accidental coincidences. If the coincidence data are to accurately reflect the intensity of each transition, one must remove the angular dependence from the data. When two detectors are located at angles of 0° and 110° with respect to the beam line, the average of the two coincidence areas associated with each pair of transitions is proportional to the true coincidence intensity, independent of the spin changes, to within 5%. This choice of angles also gives good sensitivity for the DCO analysis described below. Accordingly, the three detectors were located at angles of +110°, 0°, and −110° relative to the beam axis. With the high data rate and these precautions, the coincidence measurements provide γ-ray intensity and energy values which have similar accuracy to that usually obtained from singles measurements.

The detectors were located approximately 2.5 cm from the target. Compton scattering of γ rays from one detector into another was reduced by placing lead absorbers inside and outside of the target chamber. The time pickoffs from the three detectors were multiplexed through one time-to-amplitude converter. Two single-channel analyzer gates were set on the output of the time-to-ampli-

tude converter so the events could be identified as either true-plus-chance or chance.

The digital gates were set on spectra like that in Fig. 1 which show all the γ rays in one detector in coincidence with any γ ray in the other two detectors. Only the ^{106}Cd γ rays are labeled in Fig. 1, but most other peaks have also been positively identified as coming from one of the contaminant reactions. Sample gated spectra are shown in Fig. 2. These gates do not represent the strongest lines in the spectra but are typical and do indicate the average quality of the coincidence data.

The results of γ-ray angular distributions, γ-γ directional correlations, and γ-ray linear polarization measurements were combined to make angular momentum and parity assignments. The angular distributions included nine angles from +90° to −30° with respect to the beam axis, in order to eliminate systematic errors and thus permit the accurate determination of angular distribution coefficients.[7] The linear polarization measurements were made in collaboration with Lee, Stromswold, and Elliot of the Johns Hopkins University using a Ge(Li) two-crystal Compton polarimeter. The experimental description and results of this measurement (only summarized here) have been published previously.[8]

Angular distribution measurements are not reliable unless the γ ray of interest is uncontaminated in the singles spectra. The three detectors in the coincidence experiment were arranged so the directional correlation from orientated nuclei (DCO) technique[9] could be used to determine angular momentum changes for unresolved transitions. The basic information unit is the ratio of the two coincidence intensities N_{12} and N_{21}, where N_{12} is the number of times γ_1 is detected in detector x with γ_2 in detector y.

$$R_{\mathrm{DCO}} = \frac{N_{12}}{N_{21}}$$

This ratio can be calculated for various multipolarities and the mixing ratios for both γ_1 and γ_2. The ideal case is that where γ_2 is a quadrupole

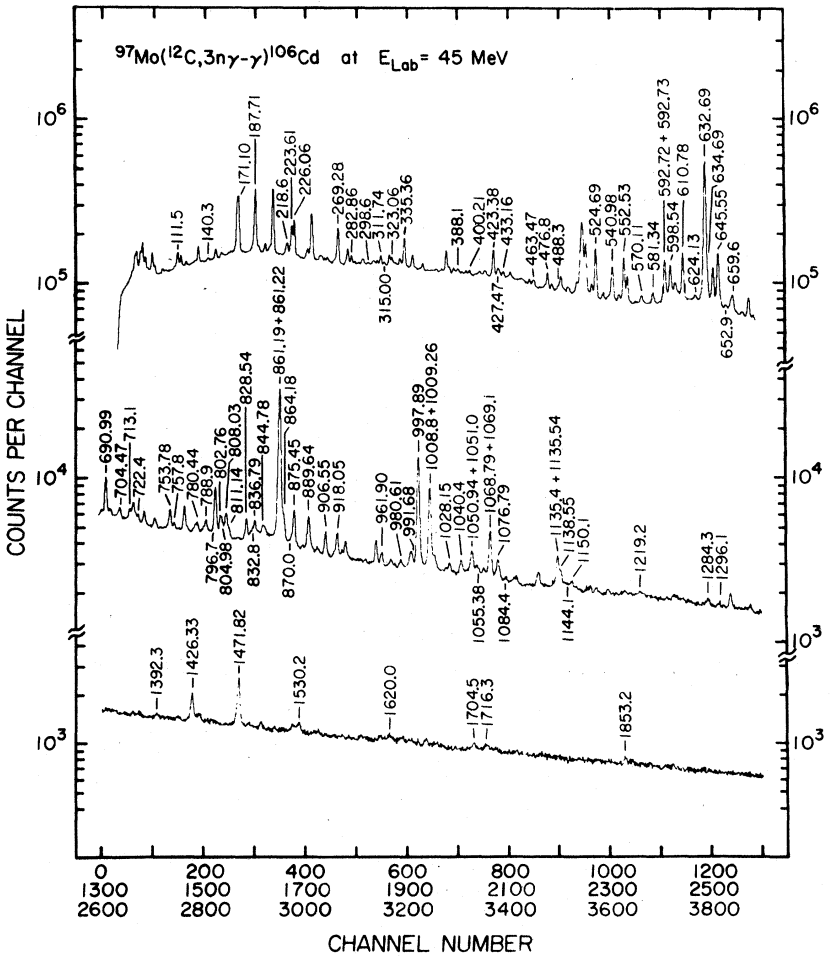

FIG. 1. Typical coincidence projection spectrum for ^{106}Cd. Only γ rays assigned to ^{106}Cd are labeled. Many peaks are multiplets, so Table I should be consulted. The data were accumulated during 35 hours of beam time at an average rate of 1600 cts/s. The detectors were positioned at 0°, +100°, and −100°. The spectrum shown is from the +100° detector stored in the XADC and represents the coincidence projection spectrum of the +100° and −100° pair.

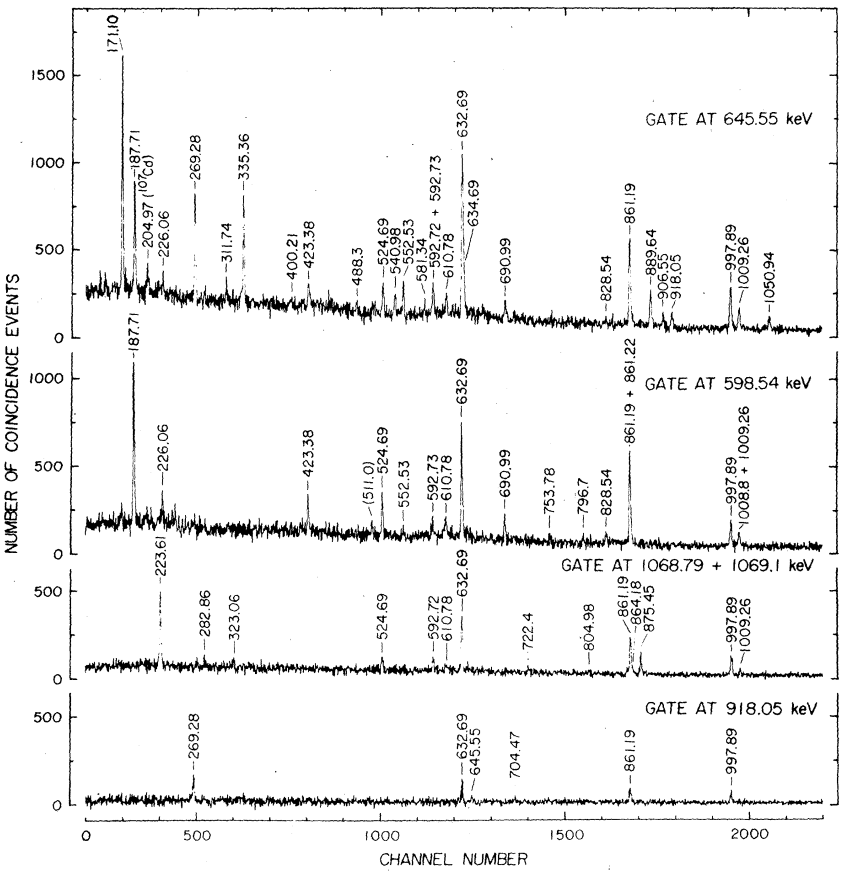

FIG. 2. Typical gated coincidence spectra from the ^{97}Mo(^{12}C, $3n\gamma$-γ)^{106}Cd reaction at 45 MeV.

transition, since the ratio is easily interpreted. All ratios where the same γ_1 is in coincidence with different quadrupole transitions should be equal, so several ratios can be combined for better statistical accuracy. If γ_2 is not a quadrupole, a corrected ratio can be calculated if the ratio involving γ_2 and a known quadrupole transition γ_3 has also been measured. Thus, a large number of DCO ratios can be suitably combined to construct an average ratio for γ_1 compared to quadrupole transitions, called an average DCOQ ratio. Details of this procedure are described in Ref. 4.

The analysis of angular distribution and DCOQ measurements is complicated by the nuclear deorientation that occurs when particles or unobserved γ rays are emitted. As shown previously,[10] this problem can be handled with a systematic analysis of consecutive transitions. Thus these techniques can be used to make unambiguous angular momentum assignments.

III. LEVEL SCHEME

Our proposed level scheme for ^{106}Cd is shown in Figs. 3 and 4. The 997.89-861.19-632.69-keV, $6^+ \rightarrow 4^+ \rightarrow 2^+ \rightarrow 0^+$ yrast γ-ray cascade of ^{106}Cd is well known from previous experiments.[6,11,12] Our assignment of γ rays to ^{106}Cd is then based upon the observation of coincidences with one or more of these γ rays. Table I lists 93 γ rays assigned to ^{106}Cd in this manner. The energies of uncontaminated lines are those adopted from the singles measurements. The energies of other γ rays were determined from peak centroids which were isolated in various gated coincidence spectra. Also listed in Table I are the relative intensities of ^{106}Cd and some contaminant γ rays from both singles and coincidence measurements using the ^{97}Mo(^{12}C, $3n\gamma$)^{106}Cd reaction at 45 MeV. The adopted γ-ray intensities in column 4 are weighted averages of the singles and coincidence intensities in the case of clean lines of just the coincidence intensities for contaminated lines.

A comparison of the singles and coincidence intensities listed in Table I illustrates the value of precise coincidence measurements. The uncertainties of coincidence intensities are the same order or smaller than the uncertainties of singles intensities. Thus contaminated lines can be identified and there are many cross checks on the placement of transitions in the decay scheme. The intensity of each transition must be consistent for all gates

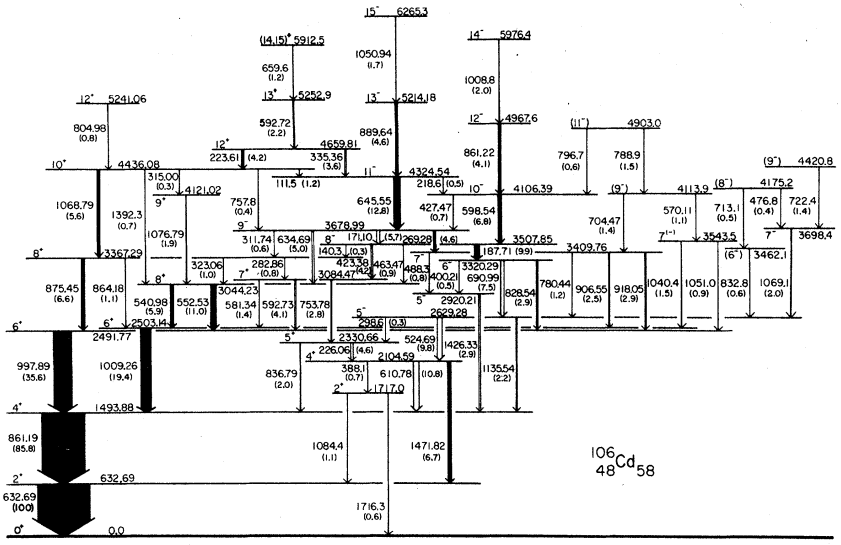

FIG. 3. Decay scheme of ^{106}Cd showing majority of states. Some additional states are shown in Fig. 4. The relative intensities given in parentheses are those from the ^{97}Mo(^{12}C, $3n\gamma$)^{106}Cd reaction at 45 MeV and represent total decay intensities where (theoretical) corrections for internal conversions of greater than 1% have been included. The widths of the arrows are proportional to these decay intensities. Darkened arrows indicate $E2$ transitions.

that involve that γ ray. Energy sums and difference are included in the analysis, but in no case were transitions placed solely on that basis.

The experimental angular distributions were described by the standard relation

$$W(\theta)=A_0Q_0\left[1+A_{22}\,\frac{Q_2}{Q_0}\,P_2(\cos\theta)+A_{44}\,\frac{Q_4}{Q_0}\,P_4(\cos\theta)\right],$$

where the Q_k are solid angle correction factors, A_0 is a measure of the total γ-ray intensity, and the effect of deorientation is included in the distribution coefficients by the parameters α_k, defined

$$A_{kk}=\alpha_k A^0_{kk}.$$

The A^0_{kk} values are readily calculated for given spin changes and mixing ratios[13]; thus if the α_k values are known, the multipolarity and mixing ratio of a transition can be determined. For pure $E2$ transitions the α_k values can be determined directly from the angular distribution measurement. The α_k values for all mixed transitions were then calculated from those of neighboring $E2$ transitions, taking into account any deorientation owing to γ-ray emission.[10] The results of this analysis for transitions that were adequately resolved following the ^{96}Mo(^{13}C, $3n\gamma$)^{106}Cd reaction at 45 MeV are presented in Table II. Since this reaction is different from that used to take the coincidence data, the observed relative γ-ray intensities are also included in column 2.

The linear polarizations $P_{\rm exp}$ were measured for the cleanest and strongest γ rays following the ^{94}Zr(^{16}O, $4n\gamma$)^{106}Cd reaction at 63 MeV. From measured angular distribution (a.d.) coefficients using

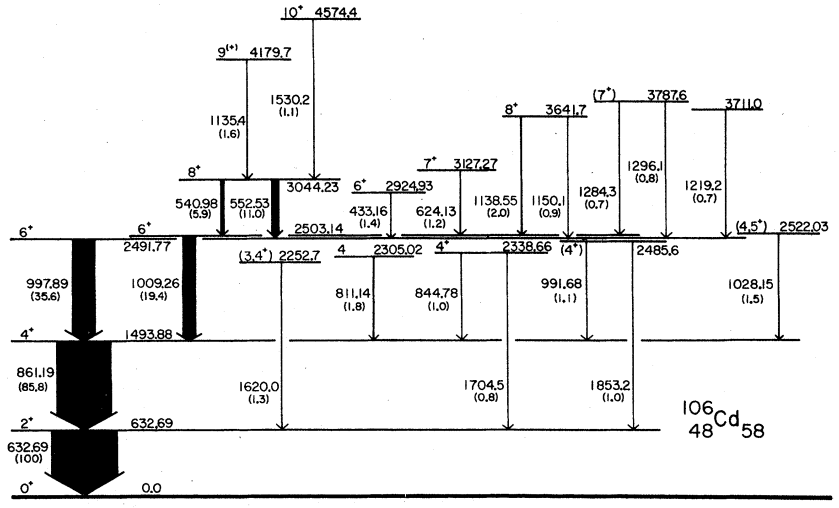

FIG. 4. Decay scheme of positive-parity states in ^{106}Cd showing additional states not shown in Fig. 3. Asterisks indicate states where not all decay γ rays are shown (see Fig. 3).

TABLE I. Intensity analysis for γ rays emitted following the ^{97}Mo(^{12}C, $3n\gamma$)^{106}Cd reaction at 45 MeV.

Energy (keV)	Relative γ-ray intensity Singles	Coincidence	Adopted	Unresolved contaminants[a] Energy	origin	intensity[b]
111.5[c,d]	35.6(16)	10.2(21)	10.2(21)	110.00	^{19}F	e
				110.53	^{106}Ag	e
140.3(4)[d]	6.1(13)	2.4(11)	2.4(11)	139.88	^{75}Ge^{m}	e
171.10(5)	53.4(18)	49.4(15)	51.4(12)			
187.71(5)[d]	93.1(28)	82.9(19)	82.9(19)	185.94	^{103}Pd	9.4(6)
218.6(5)[d]	13.1(10)	4.3(10)	4.3(10)	218	^{107}Ag	2.4(7)
				219	^{106}Ag	8.0(4)
223.61(5)[d]	39.8(15)	37.9(16)	37.9(16)	222	^{107}Ag	3.3(5)
226.06(5)[d]	43.1(18)	41.1(16)	41.1(16)	227.5	^{106}Ag	1.7(5)
269.28(7)[d]	86.5(33)	43.9(22)	43.9(22)	268.71	^{197}Au	6.9(14)
				268.75	^{197}Au	28.4(6)
				270	^{106}Ag	7.2(4)
282.86(20)[d]	14.3(19)	8.3(13)	8.3(13)	283	(^{197}Au)	2.4(5)
298.6[c]		3.0(11)	3.0(11)			
311.74(25)[d]	9.6(11)	5.8(16)	5.8(16)	312	^{107}Ag	4.5(9)
315.00(30)	1.9(6)	4.1(13)	3.0(7)			
323.06(10)	11.4(8)	9.0(8)	10.2(6)			
335.36(5)	35.7(13)	36.1(16)	35.9(10)			
388.1(4)	8.2(12)	6.1(11)	7.1(18)			
400.21(30)	3.5(12)	5.5(17)	4.5(10)			
423.38(5)	42.9(19)	41.2(21)	42.0(14)			
427.47(30)[d]	14.1(11)	6.9(19)	6.9(19)	428	^{97}Mo	6.2(6)
				428	(^{106}Ag)	1.6(4)
433.16(7)[d]	16.7(12)	13.9(15)	13.9(15)	433	^{106}Ag	2.5(5)
463.47(15)	8.8(19)	8.4(20)	8.6(14)			
476.8(4)[d]	48.3(14)	4.3(14)	4.3(14)	476.70	^{103}Pd	46.5(20)
488.3(10)[d]	25.3(13)	8.3(16)	8.3(16)	490.2	^{106}Ag	12.6(5)
				491	^{106}Ag	3.4(8)
524.69(5)	95.6(28)	100.9(31)	98.2(21)			
540.98(7)[d]	81.8(22)	58.7(29)	58.7(29)	541.0	^{103}Pd	3.5(8)
				541.2	^{106}Ag	17.4(11)
552.53(5)	115.2(27)	104.4(30)	109.8(20)			
570.11(15)[d]	17.6(18)	10.8(23)	10.8(15)	570	^{207}Pb	e
581.34(10)	14.7(14)	13.8(18)	14.2(11)			
592.72(15), 592.73(7)	64.7(25)	21.7(13)	22.3(14)			
		39.7(21)	40.8(22)			
598.54(7)	68.0(25)	68.9(24)	68.4(17)			
610.78(5)	107.1(33)	109.8(35)	108.5(24)			
624.13(20)	11.6(21)	11.7(29)	11.6(18)			
632.69(5)	≡1000	f	≡1000			
634.69(15)	[67.9(19)][g]	49.8(36)	49.8(36)			
645.55(5)	133.9(30)	122.0(34)	127.9(23)			
652.9(4)[h]	8.0(21)	15.4(25)	11.7(16)			
659.6(5)[d]	35.5(17)	12.4(17)	12.4(17)	660.13	^{103}Pd	22.2(9)
690.99(5)	76.7(22)	73.3(27)	75.0(17)			
704.47(20)	11.9(22)	15.4(21)	13.7(15)			
713.1[c]	24.6(20)	5.3(25)	5.3(25)	714.00	^{103}Pd	25.4(14)
722.4(4)	16.4(19)	11.7(22)	14.1(15)			
753.78(8)	30.3(16)	26.4(22)	28.4(13)			
757.8(10)[d]	11.3(20)	3.8(12)	3.8(12)	758	(^{97}Mo)	3.4(12)
780.44(10)	11.9(16)	12.4(22)	12.2(14)			
788.9(4)[d]	29.0(26)	14.6(30)	14.6(30)	787	^{97}Mo	8.7(14)
796.7(10)[d]	90.6(25)	6.2(16)	6.2(16)	797.04	^{104}Pd	4.0(14)
				798.14	^{107}Cd	82.9(20)
802.76(20)[h,d], 804.98(25)	58.8(24)	13.2(28)	13.2(28)	802.46	^{104}Pd	5.8(13)
		8.4(21)	8.4(21)	803	^{106}Ag	2.3(7)
				804	^{107}Cd	12.5(15)
				804	^{107}Ag	3.3(16)
				804	^{206}Pb	e
				805	^{97}Mo	6.0(15)

TABLE I. (*Continued*)

Energy (keV)	Relative γ-ray intensity Singles	Coincidence	Adopted	Unresolved contaminants[a] Energy origin intensity[b] (keV)		
808.03(20)[d,h]	45.3(26)	11.5(25)	11.5(25)	808.3	i	8.9(16)
				808.4	^{107}Ag	7.5(23)
				808.93	^{107}Cd	12.2(19)
				809.33	^{103}Pd	5.8(17)
811.14(10)	20.2(25)	15.4(33)	17.8(21)			
828.54(7)	27.7(16)	30.1(15)	28.9(11)			
832.8(10)[d]	7.8(16)	6.0(17)	6.0(17)	833	(^{97}Mo)	2.8(12)
836.79(7)	19.4(20)	21.2(27)	20.3(17)			
844.78(20)	10.1(16)	10.6(27)	10.4(16)			
861.19(5)	878 (17)	878 (8)	858 (8)			
861.22(15)		41.7(11)	40.8(11)			
864.18(15)[d]	[59.4(17)][g]	10.7(10)[j]	10.7(10)	864	^{107}Ag	e
870.0(20)[h]	7.6(11)	9.3(26)	8.5(14)			
875.45(5)	66.7(22)	65.7(23)	66.2(16)			
889.64(7)	50.3(24)	41.9(29)	46.1(19)			
906.55(5)	24.4(24)	25.9(16)	25.1(14)			
918.05(5)	29.8(15)	28.7(12)	29.3(10)			
961.90(20)[d,h]	15.7(15)	8.3(24)	8.3(24)	961.02	^{107}Cd	3.4(15)
				962	(^{97}Mo)	4.4(14)
980.61(30)[h]	6.5(16)	6.6(27)	6.5(16)			
991.68(30)	27.5(19)	10.5(33)	10.5(33)	989.94	^{107}Cd	12.5(10)
				989	^{106}Ag	5.0(8)
997.89(5)	351 (7)	360 (6)	356 (5)			
1008.8(4)	209 (5)	20.6(19)	20.2(19)			
1009.26(7)		197.9(33)	193.6(32)			
1028.15(30)[d]	19.9(16)	15.4(25)	15.4(25)	1028	k	6.4(15)
1040.4(4)[d]	21.5(19)	14.7(23)	14.7(23)	1040	(^{97}Mo)	4.9(18)
1050.94(25)[d]	33.1(21)	17 (5)	17 (5)	1051.0	^{107}Cd	7.7(20)
1051.0(5)		9 (4)	9 (4)	1051	(^{97}Mo)	6.1(18)
1055.38(25)[d,h]	17.2(18)	11 (4)	11 (4)	1055	^{106}Ag	8.8(15)
1068.79(7)	75.9(25)	55.9(21)	56.1(21)			
1069.1(5)		19.4(17)	19.5(17)			
1076.79(15)[d]	24.7(23)	18.9(25)	18.9(25)	1076.01	^{107}Cd	7.8(14)
1084.4(4)[d]	4.7(25)	10.8(23)	10.8(23)	1085	^{97}Mo	4.5(13)
1135.4(4)	37.6(16)	15.7(18)	15.7(18)			
1135.54(20)		22.0(10)	22.0(10)			
1138.55(15)	18.2(12)	21.9(21)	20.1(12)			
1144.1(10)[h]	9.8(16)	8.8(20)	9.3(13)			
1150.1(4)[d]	10.5(15)	9.3(17)	9.3(17)	1147.66	^{107}Cd	3.2(12)
1219.2(10)	4.0(23)	9.3(25)	6.7(17)			
1284.3(10)	7.1(17)	7.7(18)	7.4(12)			
1296.1(10)		7.7(16)	7.7(16)			
1392.3(5)	2.2(21)	11.0(37)	6.6(21)			
1426.33(7)	27.2(19)	30.1(20)	28.6(14)			
1471.82(7)	68.6(22)	64.7(31)	66.7(19)			
1530.2(4)	10.5(19)	10.5(20)	10.5(14)			
1620.0(10)	11.1(20)	15.3(27)	13.2(17)			
1704.5(20)	9.8(23)	5.8(27)	7.8(18)			
1716.3(10)	6.5(23)	e	6.5(23)			
1853.2(10)	10.2(20)	10.4(23)	10.3(16)			

[a] Parentheses indicate that the listed contaminant is suggested by the coincidence data but its identification is not absolutely certain.

[b] Contaminant intensities were determined from the coincidence data in the manner of column 3.

[c] Energy determined from decay scheme.

[d] Multiplet with one or more member being a contaminant.

[e] Ground-state transition whose intensity cannot be determined from the coincidence data.

[f] The 632.69-keV γ ray is a ground-state transition and therefore an intensity cannot be extracted from the coincidence data. The coincidence to singles ratio that is determined, however, assumes this transition intensity to be 1000 in singles.

[g] A large systematic error in the peak fitting caused by a nearby very intense peak is believed to be present in the intensity value listed. The value is therefore not used.

TABLE I. (*Continued*)

[h] Not placed in decay scheme.
[i] Intensity listed is from observed coincidence with 603-keV γ ray. Contaminant is unknown.
[j] Determined from the branching ration of the 3367.29-keV state extracted from the 1068.79-keV coincidence gate and from the adopted intensity of the 875.45-keV γ ray.
[k] Intensity listed is from observed coincidences with the 603- and 892-keV γ rays. Contaminant is unknown.

TABLE II. Angular distribution analysis for ^{106}Cd γ rays following the ^{96}Mo(^{13}C, $3n\gamma$)^{106}Cd reaction at 45 MeV. The attenuation coefficients listed for $E2$ transitions have been calculated using experimental and theoretical A_{22} and A_{44} values; all other attenuation coefficients are those that have been used to extract γ-ray multipole mixing rations. Intensities listed represent total peak intensities. Note that ^{97}Mo Coulomb excitation γ rays that were present in the coincidence data will not be present here.

E_γ (keV)	I_γ	$I_i^\pi \rightarrow I_f^\pi$	A_{22}	A_{44}	α_2	α_4	Mixing ratio[a]
171.10	90.7(24)	$9^- \rightarrow 8^-$	0.000(15)	0.035(14)	0.70(4)	0.38(5)	$0.14 \leq \delta \leq 0.16$
187.71[b]	138.6(30)	$8^- \rightarrow 6^-$	0.303(10)	−0.075(10)	0.706(23)	0.38(5)	
223.61[b]	58.1(21)	$12^+ \rightarrow 10^+$	0.227(12)	−0.043(16)	0.562(30)	0.27(10)	
226.06[b]	52.0(19)	$5^+ \rightarrow 4^+$	−0.790(26)	0.047(26)	0.68(4)	0.35(4)	$-0.70 \leq \delta \leq -0.47$
269.28[c]	151 (5)	$9^- \rightarrow 7^-$	0.110(10)	−0.052(13)			
282.86[b]	11.0(9)	$8^+ \rightarrow 7^+$	−0.18(6)	0.02(10)	0.63(4)	0.27(4)	$-0.08 \leq \delta \leq 0.04$
311.74[c]	13.7(10)	$9^- \rightarrow 8^+$	−0.22(6)	−0.19(8)	0.70(4)	0.38(5)	$-0.06 \leq \delta \leq 0.05$[d]
315.00	5.0(9)	$10^+ \rightarrow 9^+$	−0.52(16)	−0.14(21)	0.61(4)	0.26(4)	$-0.14 \leq \delta \leq -0.6$
323.06	13.4(10)	$8^+ \rightarrow 8^+$	0.30(5)	−0.06(7)	0.63(4)	0.27(4)	$-0.21 \leq \delta \leq 0.25$
335.36	54.4(24)	$12^+ \rightarrow 11^-$	−0.221(26)	0.000(34)	0.562(30)	0.27(10)	$-0.08 \leq \delta \leq -0.030$
388.1	7.9(18)	$4^+ \rightarrow 2^+$	0.51(8)	0.11(12)			
423.38	55.4(19)	$8^- \rightarrow 7^+$	−0.271(20)	0.042(26)	0.706(23)	0.38(5)	$-0.06 \leq \delta \leq -0.025$
427.47[c]	13.5(10)	$10^- \rightarrow 9^-$	−0.61(9)	0.25(12)	0.787(39)	0.41(5)	$\delta \approx -0.9$[e]
433.16[c]	17.1(11)	$6^+ \rightarrow 6^+$	0.17(9)[f]	0.09(9)[f]	0.65(4)	0.28(4)	$-0.45 \leq \delta \leq -0.12$
463.47	11.5(14)	$8^- \rightarrow 8^+$	0.42(10)	0.00(15)	0.706(23)	0.38(5)	$-0.11 \leq \delta \leq 0.6$
524.69	118.6(33)	$5^- \rightarrow 4^+$	−0.272(14)	0.000(16)	0.641(30)	0.29(4)	$-0.060 \leq \delta \leq -0.031$
540.98[c]	98.2(27)	$8^+ \rightarrow 6^+$	0.333(35)[g]	−0.098(34)[g]	0.78(8)	0.49(17)	
552.53	126.1(32)	$8^+ \rightarrow 6^+$	0.359(12)	−0.075(15)	0.837(28)	0.38(8)	
570.11	11.3(17)	$(9^-) \rightarrow 7^{(-)}$	0.08(14)	0.38(21)			
581.34	20.8(11)	$7^+ \rightarrow 6^+$	−0.44(5)	−0.01(7)	0.709(30)	0.34(4)	$-0.21 \leq \delta \leq -0.12$
592.72 592.73	94.8(33)	$\begin{cases} 13^+ \rightarrow 12^+ \\ 7^+ \rightarrow 6^+ \end{cases}$	−0.502(17)	0.015(18)	$\begin{cases} 0.83(4) \\ 0.709(30) \end{cases}$	0.50(5) 0.34(4)	$-0.05 \leq \delta \leq -0.02$[h] $\delta \approx -0.4$[h]
598.54	88.6(35)	$10^- \rightarrow 8^-$	0.326(16)	−0.041(22)	0.787(39)	0.23(12)	
610.78	113.4(35)	$4^+ \rightarrow 4^+$	0.116(15)	0.033(21)	0.584(30)	0.21(4)	$-0.38 \leq \delta \leq -0.30$
624.13	12.4(14)	$7^+ \rightarrow 6^+$	−0.16(8)	0.10(15)	0.71(4)	0.34(5)	$-0.022 \leq \delta \leq 0.10$
632.69	≡1000	$2^+ \rightarrow 0^+$	0.244(6)	−0.051(6)	0.342(8)	0.0298(35)	
634.69	80 (5)	$9^- \rightarrow 8^+$	−0.262(32)	−0.036(39)	0.70(4)	0.38(5)	$-0.066 \leq \delta \leq -0.010$
645.55	181 (5)	$11^- \rightarrow 9^-$	0.293(10)	−0.080(12)	0.718(25)	0.48(7)	
652.9[i]	12.6(18)		0.47(12)	0.05(17)			
690.99	86.1(35)	$6^- \rightarrow 5^-$	0.504(17)	0.117(19)	0.666(30)	0.31(4)	$0.64 \leq \delta \leq 0.78$
704.47	20.6(14)	$(9^-) \rightarrow 7^-$	0.07(6)	−0.14(9)			
753.78	31.9(19)	$7^+ \rightarrow 5^+$	0.197(28)	−0.016(39)	0.45(6)	0.07(17)	
788.9	22.8(16)	$(11^-) \rightarrow (9^-)$	0.29(5)	−0.01(7)	0.71(12)	0.1(4)	
811.14	18.2(16)	$4 \rightarrow 4^+$	0.27(9)	−0.03(11)	0.58(4)	0.21(4)	$-0.22 \leq \delta \leq 0.22$
828.54	39.5(24)	$6^- \rightarrow 6^+$	0.34(4)	−0.01(6)	0.666(30)	0.31(4)	$-0.09 \leq \delta \leq 0.25$
832.8	8.0(10)	$(6^-) \rightarrow 5^-$	0.23(16)	0.01(22)	0.67(4)	0.31(5)	$0.20 \leq \delta \leq 0.5$
836.79	26.9(26)	$5^+ \rightarrow 4^+$	−0.46(5)	0.04(8)	0.68(4)	0.35(4)	$-0.23 \leq \delta \leq -0.13$
844.78	23.6(24)	$4^+ \rightarrow 4^+$	0.26(5)	−0.11(6)	0.58(4)	0.21(4)	$-0.16 \leq \delta \leq 0.06$ or $0.8 \leq \delta \leq 1.3$[j]
861.19 861.22[k]	925 (8)	$\begin{cases} 4^+ \rightarrow 2^+ \\ 12^- \rightarrow 10^- \end{cases}$	0.260(7)	−0.056(8)	0.510(14)	0.153(22)	
864.18[3]	32.0(19)	$8^+ \rightarrow 6^+$	0.497(39)	−0.22(5)			
870.0[i]	23.6(22)		0.00(6)	0.19(9)			
875.45	80.4(35)	$8^+ \rightarrow 6^+$	0.260(17)	−0.040(23)	0.61(4)	0.20(12)	
889.64	74.9(33)	$13^- \rightarrow 11^-$	0.303(16)	−0.076(22)	0.76(4)	0.48(14)	
906.55	36.6(24)	$7^- \rightarrow 6^+$	−0.23(4)	−0.02(5)	0.695(30)	0.34(4)	$-0.045 \leq \delta \leq 0.018$
918.05	37.7(18)	$7^- \rightarrow 6^+$	−0.245(36)	−0.01(5)	0.695(30)	0.34(4)	$-0.052 \leq \delta \leq 0.005$

TABLE II. (*Continued*)

E_γ (keV)	I_γ	$I_i^\pi \rightarrow I_f^\pi$	A_{22}	A_{44}	α_2	α_4	Mixing ratio[a]
980.61[i]	11.9(16)		−0.02(11)	−0.04(18)			
997.89	387 (5)	$6^+ \rightarrow 4^+$	0.287(8)	−0.060(8)	0.631(18)	0.248(33)	
1008.8[k] / 1009.26	227 (4)	$14^- \rightarrow 12^-$ / $6^+ \rightarrow 4^+$	0.272(10)	−0.046(11)	0.598(22)	0.19(5)	
1028.15[c]	14.2(13)	$(4,5^+) \rightarrow 4^+$	0.19(9)	−0.19(12)			
1040.4	12.0(10)	$7^{(-)} \rightarrow 6^+$	−0.17(10)	0.10(13)	0.70(4)	0.34(5)	$-0.05 \leq \delta \leq 0.11$
1050.94[c] / 1051.0[c]	35.2(23)	$15^- \rightarrow 13^-$ / $7^{(-)} \rightarrow 6^+$	0.208(34)	−0.11(5)			
1055.38[c,i]	16.1(14)		0.58(13)	−0.14(17)			
1068.79 / 1069.1	91.5(35)	$10^+ \rightarrow 8^+$ / $7^- \rightarrow 5^-$	0.252(17)	−0.065(23)	0.56(4)[m] / 0.70(9)[m]	0.26(10)[m] / 0.55(23)[m]	
1076.79[c]	26.5(30)	$9^+ \rightarrow 8^+$	0.23(18)[n]	0.01(6)[n]	0.70(5)	0.43(6)	$0.18 \leq \delta \leq 0.5$
1135.4 / 1135.54	45.7(25)	$9^{(+)} \rightarrow 8^+$ / $5^- \rightarrow 4^+$	−0.195(31)	−0.05(4)	0.70(5) / 0.641(30)	0.43(6) / 0.29(4)	$0.00 \leq \delta \leq 0.06$[o] $\delta \approx 0.0$[o]
1138.55	21.2(13)	$8^+ \rightarrow 6^+$	0.35(5)	−0.30(6)	0.82(12)	1.5(3)	
1144.1[i]	7.0(25)		1.28(13)	−0.37(18)			
1150.1[c]	9.0(30)	$8^+ \rightarrow 6^+$	0.38(13)	0.06(18)			
1284.3	11.0(32)	$(7^+) \rightarrow 6^+$	−0.01(13)	−0.13(19)	0.67(5)	0.37(6)	$0.07 \leq \delta \leq 0.22$
1296.1	6.0(25)	$(7^+) \rightarrow 6^+$	0.17(25)	0.02(34)	0.67(5)	0.37(6)	$0.07 \leq \delta \leq 0.6$
1426.33	27.7(16)	$5^- \rightarrow 4^+$	−0.13(4)	−0.13(5)	0.64(4)	0.29(4)	$0.035 \leq \delta \leq 0.09$
1471.82	68.2(31)	$4^+ \rightarrow 2^+$	0.261(19)	−0.016(26)	0.512(37)	0.04(7)	
1530.2	12.0(15)	$10^+ \rightarrow 8^+$	0.38(10)	−0.34(14)	0.92(24)	1.9(9)	

[a] Mixing ratios are believed to be good at one standard deviation. The sign convention is that of Krane and Steffen.
[b] Contaminants are too weak (< 10%) to significantly affect results.
[c] Contaminants are strong enough (> 10% but < 50%) to affect results. Trend in anisotropy can still be seen, however.
[d] Range if corrected for a 44% $M1$ ^{107}Ag contamination.
[e] Approximate value if corrected for a 33% $M1$ (^{106}Ag) contamination.
[f] Corrected for a 15% $M1$ ^{106}Ag contamination. Uncorrected values are $A_{22} = 0.11(5)$, $A_{44} = 0.08(7)$.
[g] Corrected for 22% $M1$ ^{106}Ag and 4% $M2$ ^{103}Pd contaminations. Uncorrected values are A_{22} 10.205(15), $A_{44} = -0.078(24)$.
[h] If both $\delta \approx -0.4$ from R_{DCOQ} and 53% of total intensity are assumed for the 592.73-keV γ ray, then $A_{22} = -0.29(4)$, $A_{44} = 0.00(5)$ for the 592.72-keV γ ray and indicated range of δ is obtained.
[i] Not placed in decay scheme.
[j] This range of δ is favored by A_{44} value.
[k] Too weak (< 10%) to significantly affect results.
[l] Unknown amount of contamination by $E2$ 864-keV ^{107}Ag γ ray.
[m] If both $\alpha_2 = 0.56$, $\alpha_4 = 0.26$ (calculated from γ-ray feeding) and 74% of total intensity are assumed for the 1068.79-keV γ ray, then $A_{22} = 0.31(4)$, $A_{44} = -0.12(5)$ for the 1069.1-keV γ ray and the associated values of α_2 and α_4 are obtained.
[n] Corrected for a 30% $E1$ ^{107}Cd contamination. Uncorrected values are $A_{22} = 0.10(6)$, $A_{44} = 0.01(9)$.
[o] If both $\delta \approx 0.0$ from R_{DCOQ} and 58% of total intensity are assumed for the 1135.54-keV γ ray, then $A_{22} = -0.17(4)$, $A_{44} = -0.12(11)$ for the 1135.4-keV γ ray and indicated ranae of δ is obtained.

this same reaction and beam energy, linear polarizations $P_{a.d.}$ were calculated for possible spin changes and mixing ratios assuming no parity change.[8] For the correct choice of spin change and γ-ray mixing ratio, the ratio of P_{exp} to $P_{a.d.}$ should have a magnitude of one within error. Since the sign of the linear polarization P_{exp} is strictly determined by the change in parity caused by the transition, the sign of the ratio of P_{exp} to $P_{a.d.}$ uniquely reflects parity changes: plus one requires no parity change, minus one requires a parity change. The results of this experiment are presented in Table III. Again, this reaction is different from those already presented, so the observed relative γ-ray intensities are presented in column 2.

The DCOQ ratios for all transitions that could be isolated with sufficient statistics in the ^{97}Mo(^{12}C, $3n$)^{106}Cd coincidence measurement were determined. The results given in Table IV for transitions unresolved in the singles were used to determine their angular momentum change. Transitions that are cleanly resolved are also included to demonstrate the reliability of the DCOQ method. It should be kept in mind, however, that an angular distribution measurement is somewhat more sensitive to the multipolarity of a transition than the DCOQ ratio.

In the DCOQ analysis the experimental values are compared to a detailed calculation of the DCOQ ratio; however, there are several general guidelines for a simplified interpretation of average

TABLE III. Linear polarization results for ^{106}Cd γ rays following the ^{94}Zr(^{16}O, $4n\gamma$)^{106}Cd reaction at 63 MeV. The A_{22} and A_{44} values are from an angular distribution measurement using this same reaction. The γ-ray intensities are from the angular distribution measurement as well as singles ($\theta = 125°$) and γ-γ coincidence measurements also using the same reaction.

E_γ (keV)	I_γ	$I_i \rightarrow I_f$	A_{22}	A_{44}	$P_{a.d.}$	P_{exp}	$P_{exp}/P_{a.d.}$	Multipolarity	Mixing ratio $\delta_{a.d.}$
632.69	≡100	2→0	0.230(8)	−0.045(11)	0.365(17)	0.39(4)	1.07(12)	$E2$	
861.19[a]	77.4(9)	4→2	0.237(9)	−0.059(10)	0.371(19)	0.43(5)	1.16(15)	$E2$	
997.89	30.8(6)	6→4	0.276(14)	−0.079(17)	0.438(30)	0.55(15)	1.26(35)	$E2$	
1009.26[b]	17.2(6)	6→4	0.162(27)	−0.04(4)	0.24(5)	0.42(15)	1.8(7)	$E2$	
875.45[c]	7.0(10)	8→6	0.29(4)	−0.05(5)	0.48(9)	0.73(30)	1.5(7)	$E2$	
524.69	8.5(4)	5→4	−0.239(31)	−0.03(4)	−0.31(7)	0.36(14)	−1.2(5)	$E1$	$-0.035 \leq \delta \leq 0.017$
592.73[d]	5.0(5)	7→6	−0.61(10)	0.23(12)	−0.05(8)	−0.10(13)	2.0(40)	$M1/E2$	$-0.54 \leq \delta \leq -0.24$
610.78[e]	9.5(6)	4→4	0.134(31)	0.05(4)	0.60(19)	0.38(13)	0.63(30)	$M1/E2$	$-0.37 \leq \delta \leq -0.26$
690.99[f]	5.9(6)	6→5	f	f		−0.86(32)		$M1/E2$	

[a] The 861.22-keV ^{106}Cd γ ray, with unknown intensity (but probably <6), is also present in results.
[b] The 1008.8-keV ^{106}Cd γ ray, with unknown intensity (but probably <2), is also present in results.
[c] A 41% contamination by an 875.46-keV $E2$ ^{108}Cd γ ray is present in results (except intensity value).
[d] The 592.72-keV ^{106}Cd γ ray, with unknown intensity (but probably ≈2), is also present in results.
[e] See text for further discussion. A 36% contamination by a 611.89-keV $E2$ ^{104}Pd γ ray is present in results (except intensity value).
[f] Contaminated severely in singles by 691-keV ^{72}Ge(n,n'). The lack of Compton scattering from the 691-keV $E0$ transition in ^{72}Ge and the coincidence requirement, however, allowed determination of P_{exp}. The P_{exp} value is consistent with a large positive mixing ratio.

TABLE IV. Average DCOQ ratios from the ^{97}Mo(^{12}C, $3n\gamma$)^{106}Cd coincidence data for many of the transitions assigned to ^{106}Cd. The detector angles were 0° and ±100°.

E_γ (keV)	$I_i^\pi \rightarrow I_f^\pi$	R_{DCOQ}	Mixing ratio[a] From DCOQ	Mixing ratio[a] From a.d.
		$\Delta I = -1$ transitions with $\delta > 0$		
171.10	$9^- \rightarrow 8^-$	1.40(5)	$0.13 \leq \delta \leq 0.17$	$0.14 \leq \delta \leq 0.16$
690.99	$6^- \rightarrow 5^-$	0.617(20)	$0.94 \leq \delta \leq 1.5$	$0.64 \leq \delta \leq 0.78$
1076.79[b]	$9^+ \rightarrow 8^+$	0.89(18)	$0.30 \leq \delta \leq 0.6$	$0.18 \leq \delta \leq 0.5$
		$\Delta I = -1$ transitions with $\delta < 0$		
226.06[b]	$5^+ \rightarrow 4^+$	3.36(28)	$-0.31 \leq \delta \leq -0.24$	$-0.70 \leq \delta \leq -0.47$
282.86[b]	$8^+ \rightarrow 7^+$	3.1(8)	$-0.43 \leq \delta \leq -0.12$	$-0.08 \leq \delta \leq 0.04$
427.47[c]	$10^- \rightarrow 9^-$	4.3(26)	$-0.4 \leq \delta \leq 0.09$	$\delta \approx -0.9$
581.34	$7^+ \rightarrow 6^+$	4.2(15)	$-0.44 \leq \delta \leq -0.10$	$-0.21 \leq \delta \leq -0.12$
592.73[b]	$7^+ \rightarrow 6^+$	5.3(8)	$-0.45 \leq \delta \leq -0.32$	
836.79	$5^+ \rightarrow 4^+$	3.2(10)	$-0.43 \leq \delta \leq -0.06$	$-0.23 \leq \delta \leq -0.13$
		$\Delta I = -1$ transitions with $\delta \approx 0$		
311.74[b]	$9^- \rightarrow 8^+$	1.5(4)	$0.018 \leq \delta \leq 0.29$	$-0.06 \leq \delta \leq 0.05$
335.36	$12^+ \rightarrow 11^-$	1.85(12)	$-0.09 \leq \delta \leq -0.015$	$-0.08 \leq \delta \leq -0.030$
400.21	$6^- \rightarrow 5^-$	2.2(8)	$-0.16 \leq \delta \leq 0.17$	
423.38	$8^- \rightarrow 7^+$	1.67(13)	$0.005 \leq \delta \leq 0.08$	$-0.06 \leq \delta \leq -0.025$
524.69	$5^- \rightarrow 4^+$	1.84(7)	$0.057 \leq \delta \leq 0.095$	$-0.060 \leq \delta \leq -0.031$
592.72[b]	$13^+ \rightarrow 12^+$	1.62(22)	$-0.05 \leq \delta \leq 0.11$	$-0.05 \leq \delta \leq -0.02$
624.13	$7^+ \rightarrow 6^+$	1.8(8)	$-0.09 \leq \delta \leq 0.35$	$-0.022 \leq \delta \leq 0.10$
634.69	$9^- \rightarrow 8^+$	2.10(31)	$-0.08 \leq \delta \leq 0.04$	$-0.066 \leq \delta \leq -0.010$
906.55	$7^- \rightarrow 6^+$	1.93(24)	$-0.029 \leq \delta \leq 0.08$	$-0.045 \leq \delta \leq 0.018$
918.05	$7^- \rightarrow 6^+$	1.89(19)	$-0.011 \leq \delta \leq 0.08$	$-0.052 \leq \delta \leq 0.005$
1135.4[b]	$9^{(+)} \rightarrow 8^+$	2.8(10)	$-0.15 \leq \delta \leq 0.09$	$0.00 \leq \delta \leq 0.06$
1135.54[b]	$5^- \rightarrow 4^+$	1.88(28)	$-0.05 \leq \delta \leq 0.09$	
1426.33	$5^- \rightarrow 4^+$	1.96(36)	$-0.06 \leq \delta \leq 0.11$	$0.035 \leq \delta \leq 0.09$
		$\Delta I = 0$ transitions		
323.06	$8^+ \rightarrow 8^+$	0.70(16)	$0.13 \leq \delta \leq 0.33$	$-0.21 \leq \delta \leq 0.25$
433.16[b]	$6^+ \rightarrow 6^+$	0.93(14)	$-0.21 \leq \delta \leq 0.33$	$-0.45 \leq \delta \leq -0.12$
463.47	$8^- \rightarrow 8^+$	0.99(23)	$-0.45 \leq \delta \leq 0.23$	$-0.11 \leq \delta \leq 0.6$
610.78	$4^+ \rightarrow 4^+$	0.880(34)	$-0.10 \leq \delta \leq 0.019$	$-0.38 \leq \delta \leq -0.30$
811.14	$4 \rightarrow 4^+$	1.3(6)	$-1.4 \leq \delta \leq 0.4$	$-0.22 \leq \delta \leq 0.22$
828.54	$6^- \rightarrow 6^+$	0.92(7)	$-0.09 \leq \delta \leq 0.28$	$-0.09 \leq \delta \leq 0.25$
		$\Delta I = -2$ transitions		
187.71[b]	$8^- \rightarrow 6^-$	0.972(23)		
223.61[b]	$12^+ \rightarrow 10^+$	1.05(5)		
269.28[c]	$9^- \rightarrow 7^-$	1.02(5)		
388.1	$4^+ \rightarrow 2^+$	1.02(26)		
488.3[c]	$7^- \rightarrow 5^-$	0.81(38)		
540.98[c]	$8^+ \rightarrow 6^+$	0.97(7)		
552.53	$8^+ \rightarrow 6^+$	0.934(38)		
570.11[d]	$(9^-) \rightarrow 7^{(-)}$	0.80(29)		
598.54	$10^- \rightarrow 8^-$	1.02(6)		
632.69	$2^+ \rightarrow 0^+$	0.955(13)		
645.55	$11^- \rightarrow 9^-$	1.06(4)		
704.47	$(9^-) \rightarrow 7^-$	1.15(28)		
722.4	$(9^-) \rightarrow 7^-$	1.8(5)		
753.78	$7^+ \rightarrow 5^+$	1.01(9)		
780.44	$7^- \rightarrow 5^-$	0.94(20)		
804.98[c]	$12^+ \rightarrow 10^+$	1.2(4)		
861.19[b]	$4^+ \rightarrow 2^+$	1.036(15)		
861.22[b]	$12^- \rightarrow 10^-$	0.92(16)		
875.45	$8^+ \rightarrow 6^+$	0.99(6)		
889.64	$13^- \rightarrow 11^-$	1.10(11)		
997.89	$6^+ \rightarrow 4^+$	1.025(21)		
1008.8[b]	$14^- \rightarrow 12^-$	1.09(19)		
1009.26[b]	$6^+ \rightarrow 4^+$	1.054(32)		
1050.94[c]	$15^- \rightarrow 13^-$	1.12(24)		
1068.79[b]	$10^+ \rightarrow 8^+$	0.91(10)		
1069.1[b]	$7^- \rightarrow 5^-$	1.37(33)		

TABLE IV. (*Continued*)

E_γ (keV)	$I_i^\pi \rightarrow I_f^\pi$	R_{DCOQ}	Mixing ratio[a] From DCOQ	From a.d.
1138.55	$8^+ \rightarrow 6^+$	1.25(19)		
1471.82	$4^+ \rightarrow 2^+$	1.10(14)		
1530.2	$10^+ \rightarrow 8^+$	1.5(5)		
		Other transitions		
659.6[b]	$(14,15)^+ \rightarrow 13^+$	0.91(23)	$0.27 \leq \delta \leq 0.7$[d]	
1028.15[b]	$(4,5^+) \rightarrow 4^+$	0.79(22)	$-0.23 \leq \delta \leq 1.0$[e] $0.4 \leq \delta \leq 1.2$[f]	

[a] If more than one range of mixing ratio is consistent with the DCOQ ratio, the range closest to the angular distribution value has been chosen. The mixing ratio sign convention is that of Krane and Steffen.
[b] Doublet in singles.
[c] Multiplet in singles.
[d] Applies only if $I_i = 14$.
[e] Applies only if $I_i = 4$.
[f] Applies only if $I_i = 5$.

DCOQ ratios. The DCOQ ratio is approximately equal to the ratio of the anisotropy of the two transitions. Thus, (1) $R_{DCOQ} = 1$ is characteristic (but not unique) of a $\Delta I = -2$ transition, (2) $R_{DCOQ} \simeq 2$ implies a $\Delta I = \pm 1$ pure-dipole transition (3) $R_{DCOQ} > 3$ uniquely describes a $\Delta I = \pm 1$ transition, and (4) $R_{DCOQ} < 1$ implies $\Delta I = 0$ or $\Delta I = \pm 1$.

Finally, two additional aids were used in assigning spins and parities. First, since highly mixed $M2/E1$ transitions are very unlikely, a substantial mixing ratio for any $\Delta I = 0$ or $\Delta I = \pm 1$ transition was interpreted as meaning that the transition is $E2/M1$ and hence non-parity changing. Second, the experiments measure the ΔI associated with a transition, but they are not sensitive to whether I increases or decreases. However, for states observed following (HI, xn) reactions it is frequently easy to remove this ambiguity by using the yrast argument, i.e., at a given energy, the state with highest angular momentum is preferentially populated. Thus when a transition is observed from a state with I_i to a state with I_f, it is much more likely that $I_i = I_f + \Delta I$ rather than $I_i = I_f - \Delta I$. In addition, the change in I associated with $\Delta I = 1$ transitions frequently can be determined because the unknown state is bracketed between two states of known angular momentum.

A complete summary of the combination of experimental evidence and arguments used to yield spin and parity assignments is presented in Table V. The table is organized by energy levels in ascending order. Observed transitions depopulating a particular level are identified by their energies and relative intensities. The spin and parity change for each transition (determined from Tables II, III, or IV) are given, along with the energy and predetermined spin and parity of each final state populated. On the basis of this information a spin and parity has been assigned to the energy level in question. Notice that in many cases several pieces of corroborating evidence exist. If the results for a particular transition definitely eliminate a spin possibility for the level in question, then this eliminated possibility is not considered for other depopulating transitions. For example, if the measurements for one transition are inconclusive between $\Delta I = 0$ and $\Delta I = -2$, but the results for another eliminate the $\Delta I = 0$ possibility, then only $\Delta I = -2$ is presented. The overall consistency of the decay scheme gives us considerable confidence that all of the unparenthesized spin and parity assignments are correct.

The ^{106}Cd decay scheme can be divided into two distinct parts, one having positive parity and one having negative parity. Because most of the transitions connecting the negative-parity states to the positive-parity states are either weak or contaminated, all negative-parity assignments ultimately depend upon the nature of the clean and relatively strong 524.69-keV transition from the 2629.28-keV state shown in Fig. 3. As can be seen in Table III, we have unambiguously determined from its linear polarization that this transition is $E1$, and hence parity changing. Note that the other γ rays connecting negative- to positive-parity states, namely, those with energies 311.74-, 335.36-, 423.38-, 634.69-, 906.55-, 918.05-, 1040.4-, 1135.54-, and 1426.33-keV, have angular distributions ($A_{22} \simeq -0.25, A_{44} \simeq 0.00$) and DCOQ ratios ($R_{DCOQ} \simeq 2.0$) characteristic of $\Delta I = -1$, $\delta \approx 0$ transitions (i.e., consistent with pure $E1$). Note also that the 463.47- and 828.54-keV connecting γ rays have angular distributions ($A_{22} \simeq +0.40, A_{44} \simeq 0.00$) and DCOQ ratios ($R_{DCOQ} \simeq 0.90$) characteristic of $\Delta I = 0$, $\delta \approx 0$ transitions (i.e., again consistent with pure $E1$). Thus

TABLE V. Tabular presentation of level scheme. Deduced levels are arranged in ascending order of their energy. The spin and parity assigned to each level is based on the angular momentum and parity change measured for each transition depopulating the level in question to a final state whose spin and parity are known. The energy and relative intensity [from the ^{97}Mo(^{12}C, $3n\gamma$)^{106}Cd reaction at 45 MeV] of each depopulating transition are listed, along with the final state energy and spin-parity assignment justified earlier in the table. The angular momentum and parity change measured for each transition is presented, along with the type of measurement(s) used. A $\Delta I = -2$ transition is assumed to be $E2$, hence $\Delta\pi$ = No. A highly mixed $\Delta I = 0$ or -1 transition is assumed to be $E2/M1$, hence $\Delta\pi$ = No also.

Level energy (keV)	Assigned J^π	E_γ (keV)	I_γ	E_f (keV)	J_f^π	ΔJ	$\Delta\pi$	Measurement
0.00	0^+							
632.69	2^+	632.69	≡100	0.00	0^+	−2	No	a,b,c
1493.88	4^+	861.19	85.8	632.69	2^+	−2	No	a,b,c
1717.0	2^+[d]	1084.4	1.1	632.69	2^+			
		1716.3	0.65	0.00	0^+			
2104.59	4^+	388.1	0.71	1717.0	2^+		(No)	
		610.78	10.8	1493.88	4^+	0	No	a,b,c
		1471.82	6.7	632.69	2^+	−2	No	a,c
2252.7	$(3,4^+)$[d]	1620.0	1.3	632.69	2^+		(No)[e]	
2305.02	4^+[f]	811.14	1.8	1493.88	4^+	0 or −2		a,c
2330.66	5^+	226.06	4.1	2104.59	4^+	−1	No	a,c
		836.79	2.0	1493.88	4^+	−1	No	a,c
2338.66	4^+	844.78	1.0	1493.88	4^+	0		a
		1704.5	0.78	632.69	2^+		(No)	
2485.6	(4^+)[d]	991.68	1.1	1493.88	4^+			
		1853.2	1.0	632.69	2^+		(No)	
2491.77	6^+	997.89	35.6	1493.88	4^+	−2	No	a,b,c
2503.14	6^+	1009.26	19.4	1493.88	4^+	−2	No	a,b,c
2522.03	$(4,5^+)$	1028.15	1.5	1493.88	4^+	0 or −1	No[g]	c
2629.28	5^-	298.6	0.30	2330.66	5^+			
		524.69	9.8	2104.59	4^+	−1	Yes	a,b,c
		1135.54	2.2	1493.88	4^+	−1		c
2920.21	5^-[h]	1426.33	2.9	1493.88	4^+	−1		a,c
2924.93	6^+[i]	433.16	1.4	2491.77	6^+	0 or −2		a,c
3044.23	8^+	540.98	5.9	2503.14	6^+	−2	No	a,c
		552.53	11.0	2491.77	6^+	−2	No	a,c
3084.47	7^+	581.34	1.4	2503.14	6^+	−1	No	a,c
		592.73	4.1	2491.77	6^+	−1	No	a,b,c
		753.78	2.8	2330.66	5^+	−2	No	a,c
3127.27	7^+[j]	624.13	1.2	2503.14	6^+	−1		a,c
3320.29	6^-	400.21	0.45	2920.21	5^-	−1		c
		690.99	7.5	2629.28	5^-	−1	No	a,b,c
		828.54	2.9	2491.77	6^+	0		a,c
3367.29	8^+	282.86	0.83	3084.47	7^+	−1		a,c
		323.06	1.0	3044.23	8^+	0		a,c
		864.18	1.1	2503.14	6^+	(−2)	(No)	a
		875.45	6.6	2491.77	6^+	−2	No	a,b,c
3409.76	7^-	488.3	0.83	2920.21	5^-	−2	No	c
		780.44	1.2	2629.28	5^-	−2	No	c
		906.55	2.5	2503.14	6^+	−1		a,c
		918.05	2.9	2491.77	6^+	−1		a,c
3462.1	(6^-)	832.8	0.60	2629.28	5^-	(−1)	(No)	a
3507.85	8^-	140.3	0.24	3367.29	8^+			
		187.71	8.3	3320.29	6^-	−2	No	a,c
		423.38	4.2	3084.47	7^+	−1		a,c
		463.47	0.86	3044.23	8^+	0		a,c
3543.5	$7^{(-)}$[h]	1040.4	1.5	2503.14	6^+	−1		a
		1051.0	0.9	2491.77	6^+			
3641.7	8^+	1138.55	2.0	2503.14	6^+	−2	No	a,c
		1150.1	0.93	2491.77	6^+	(−2)	(No)	a
3678.99	9^-	171.10	5.1	3507.85	8^-	−1	No	a,c
		269.28	4.4	3409.76	7^-	−2	No	c
		311.74	0.58	3367.29	8^+	−1		a,c
		634.69	5.0	3044.23	8^+	−1		a,c
3698.4	7^-	1069.1	2.0	2629.28	5^-	−2	No	a,c
3711.0		1219.2	0.67	2491.77	6^+			

TABLE V. (*Continued*)

Level energy (keV)	Assigned J^π	E_γ (keV)	I_γ	E_f (keV)	J_f^π	ΔJ	$\Delta\pi$	Measurement
3787.6	(7^+)	1284.3	0.74	2503.14	6^+	(−1)	(No)	a
		1296.1	0.77	2491.77	6^+	(−1)	(No)	a
4106.39	10^-	427.47	0.69	3678.99	9^-	−1	No	a,c
		598.54	6.8	3507.85	8^-	−2	No	a,c
4113.9	(9^-) [d]	570.11	1.1	3543.5	$7^{(-)}$	(0,−1) or −2	No	a,c
		704.47	1.4	3409.76	7^-	(0,−1) or −2	No	a,c
4121.02	9^{+k}	1076.79	1.9	3044.23	8^+	−1	No	a,c
4175.2	(8^-) [d]	476.8	0.43	3698.4	7^-			
		713.1	0.53	3462.1	(6^-)		(No)	
4179.7	$9^{(+)}$	1135.4	1.6	3044.23	8^+	−1		a,c
4324.54	11^-	218.6	0.43	4106.39	10^-			
		645.55	12.8	3678.99	9^-	−2	No	a,c
4420.8	(9^-) [d]	722.4	1.4	3698.4	7^-	(−2)	(No)	c
4436.08	10^+	111.5	1.0	4324.54	11^-			
		315.00	0.30	4121.02	9^+	−1	No	a
		757.8	0.38	3678.99	9^-			
		1068.79	5.6	3367.29	8^+	−2	No	a,c
		1392.3	0.66	3044.23	8^+			
4574.4	10^+	1530.2	1.1	3044.23	8^+	−2	No	a,c
4659.81	12^+	223.61	3.8	4436.08	10^+	−2	No	a,c
		335.36	3.6	4324.54	11^-			
4903.0	(11^-) [d]	788.9	1.5	4113.9	(9^-)	(−2)	(No)	a
		796.7	0.62	4106.39	10^-			
4967.6	12^- [d]	861.22	4.1	4106.39	10^-			c
5214.18	13^-	889.64	4.6	4324.54	11^-	−2	No	a,c
5241.06	12^+ [d]	804.98	0.84	4436.08	10^+	(−2)	(No)	c
5252.9	13^+	592.72	2.2	4659.81	12^+	−1	No	a,b,c
5912.5	$(14,15)^+$ [d]	659.6	1.2	5252.9	13^+	(−1 or −2)	(No)	c
5976.4	14^- [d]	1008.8	2.0	4967.6	12^-	(−2)	(No)	c
6265.3	15^-	1050.94	1.7	5214.18	13^-	−2	No	a,c

[a] Angular distribution measurement.
[b] Linear polarization measurement.
[c] DCOQ ratio measurement.
[d] Yrast nature of reaction makes all possible lower-spin values unlikely.
[e] Applies if $J=4$.
[f] Below probable spin 5 and 6 yrast states; therefore spin 4 is most likely.
[g] Applies if $J=5$.
[h] Feeding limits parity.
[i] Below probable 6^- and 8^+ yrast states; therefore $J^\pi=6^+$ is most likely.
[j] Below probable 7^- yrast state; therefore parity is probably positive.
[k] The 315.00-keV γ ray feeding from the 4436.08-keV 10^+ state is highly mixed $E2/M1$, and therefore limits J^π to 9^+.

no inconsistencies arise in extending negative parities to connected states once a negative parity is established for the 2629.28-keV state.

Another key transition in the extension of negative parities is the highly mixed ($\delta\approx0.8$) and, hence, $6^-\rightarrow5^-$ $E2/M1$ 690.99-keV transition from the 3320.29-keV state. It is interesting to note that the analogous $6^-\rightarrow5^-$ transition in ^{108}Cd (Ref. 5), 268.39-keV, has $\delta\approx0.4$; in ^{102}Pd (Ref. 4), 439.7-keV, has $\delta\approx0.4$; in ^{104}Pd (Ref. 4), 409.46-keV, has $\delta\approx0.7$; and in ^{106}Pd (Ref. 4), 301.99-keV, has $\delta\approx0.6$. A large positive mixing ratio thus appears to be a consistent signature for this transition.

The assignment of 8^+ to the 3044.23-keV state shown in Fig. 4 is established by the depopulating $E2$ 540.98- and 552.53-keV transitions (see Tables II and IV). The only other possible assignment is 6^+ where these depopulating transitions would be very highly mixed $E2/M1$ $\Delta I=0$. However, the 9^- assignment to the 3678.99-keV state, determined independently through several different pathways, and the definite existence of the $\Delta I=-1$ 634.69-keV transition (again see Tables II and IV) between these states, makes a 6^+ assignment impossible. Furthermore, a 6^+ assignment would require the 463.47-keV transition from the 8^- 3507.85-keV state to be $\Delta I=-2$, which in turn would require positive parity for the 3057.85-keV state and hence complete inconsistency with the data.

Our 8^+ assignment to the 3044.23-keV state is in disagreement with the $4-6^\pm$ assignment made by Flanagan *et al.*[12] in their study of 6.26-min ^{106}In^m

β^+/EC decay. The 3044.23-keV state appears to be the most strongly excited state in the β decay and is most certainly the same state excited here, since the branching ratio of the 540.98- to 552.53-keV γ rays in our measurement is 0.535 ± 0.028 while in Ref. 12 it is 0.502 ± 0.036. If both the 6^+ 2491.77-keV and 6^+ 2503.14-keV states are directly fed in the β decay (which seems probable), then a 7^+ assignment to ^{106}In^m rather than 5 as suggested by Ref. 12 is the only possibility.

Other discrepancies with Ref. 12 are apparent. The branching ratio of the 610.78- to 1471.82-keV γ rays from the 2104.59-keV 4^+ state (Fig. 3) in our measurements is 1.63 ± 0.06, while Ref. 12 gives it as 0.50 ± 0.05. Also, the 388.1-keV γ ray depopulating the 2104.59-keV state was not observed. Thus it would seem that the reported[12] direct β feeding to the 4^+ 2104.59-keV state is probably erroneous, as indeed should be the case since direct β feeding would be very unlikely if ^{106}In^m is 7^+. Also the 836.79-keV γ ray from the 2330.66-keV 5^+ state (Fig. 3) was not reported in Ref. 12 even though it should have sufficient intensity to be seen. Since the 5^+ 2330.66-keV state is also unlikely to be directly populated by a 7^+ ^{106}In^m, it seems possible that several other unobserved weak transitions from higher-lying 6^+ and 7^+ states are feeding the 2330.66-keV state.

The ^{106}Cd decay scheme offers a particular challenge in the correct placement of γ rays. Six relatively intense γ-ray lines are in fact doublets with both members belonging to ^{106}Cd. For example, the 1068.79-keV γ ray can be unambiguously placed depopulating the 4436.08-keV state. However, in the 1069-keV gate (see Fig. 2) a definite coincidence is observed with the 524.69-keV γ ray, which is impossible unless an additional γ ray with an energy close to 1069-keV feeds the 2629.28-keV state. These placements are supported by their intensities determined from the coincidence data (see Table I). Of the six ^{106}Cd doublets, only one, the 632.69-634.69-keV doublet, is partially resolved in singles. A seventh ^{106}Cd γ-ray doublet with an energy of 1051-keV is in fact a member of a multiplet having two additional lines from contaminant reactions. Besides these doublets, many levels have several decay paths. Thus, the large quantity of data accumulated in the coincidence measurement and the subsequent extraction of accurate γ-ray intensities were invaluable in unravelling the decay scheme. Two interesting examples will be presented in detail.

The 1008.8-861.22-keV, $14^- \rightarrow 12^- \rightarrow 10^-$ sequence was particularly difficult to place because of the 1009.26-861.19-keV, $6^+ \rightarrow 4^+ \rightarrow 2^+$ sequence; however, the evidence is substantial. The 861-keV γ ray shows up with 8.2 units of intensity in its own gate, indicating the existence of a second 861-keV γ-ray having an intensity of 4.1 units (a division by 2 is necessary to get the actual intensity). If the 861-keV γ ray with 4.1 units of intensity is placed feeding the 4106.39-keV state as shown in Fig. 3, then the calculated 598.54-861-keV coincidence intensity should be 9.8, very close to the observed value. The 1009-keV γ ray appears in the 498.54-keV gate with 2.1 units of intensity, but from the decay scheme the maximum possible coincidence intensity with the 1009.26-keV γ ray is 0.6 units. The 1009-keV γ ray also appears in the 187.71-keV gate with 1.0 unit of intensity and in the 690.99-keV gate with 0.95 units; but in both cases coincidences with the 1009.26-keV γ ray are impossible. Finally, the 861–1009-keV coincidence intensity is 24.0 units while it should only be 19.4 if only the 861.19- and 1009.26-keV γ rays exist. A calculation using the adopted decay scheme shows that 23.3 units of intensity should be observed between the 861-1009-keV coincidence gates, almost exactly the value that is observed. Thus the 861.22- and 1008.8-keV γ ray must exist. The ordering of these two γ rays shown in Fig. 3 was finally based upon their intensities with the weaker 1008.8-keV γ ray placed above the stronger 861.22-keV γ ray.

When isolated in the 598.54-keV gate and corrected for a 60% presence of coincidences with the 861.19-keV $E2$ γ ray, a DCOQ ratio of 0.92 ± 0.19 for the 861.22-keV γ ray is obtained. Similarly, when isolated in the 187.71-, 598.54- (corrected for a 29% presence of coincidences with the 1009.26-keV $E2$ γ ray), and 690.99-keV gates, a DCOQ ratio of 1.09 ± 0.19 is obtained for the 1008.8-keV γ ray. Both values are consistent with $E2$ assignments. Finally, from the yrast nature of the reaction and since we expect from systematics[4,5] to observe the $14^- \rightarrow 12^- \rightarrow 10^-$ decay sequence with approximately the intensities of the 861.22- and 1008.8-keV γ rays, the spin assignments of 12^- to the 4967.6-keV state and 14^- to the 4976.4-keV state follow.

The 592.72-keV γ ray of the 593-keV doublet was also discovered because of the good coincidence data. The spectrum gated on the 593-keV peak shows distinct coincidences with the 223.61-, 1068.79-, and 875.45-keV γ rays and simultaneously with the 598.54-keV γ ray. (See the 598.54- and 1068.79 + 1069.1-keV gates in Fig. 2.) These coincidences are impossible for there being a single 593-keV γ ray. The intensity analysis of the coincidence data requires placement in Fig. 3 of a more intense 592.73-keV γ ray deexciting the 3084.47-keV state and a less intense 592.72-keV γ ray feeding the 4659.81-keV state. The total 593-keV peak has a very large negative anisotropy with

$A_{22} = -0.502 \pm 0.017, A_{44} = 0.015 \pm 0.018$. The DCOQ ratio of the 592.73-keV γ ray was measured to be 5.3 ± 0.8 and thus reveals that this γ ray is a highly mixed, $\delta \approx -0.4$ $\Delta I = -1$ transition. Using this information and the relative intensities of the 592.72- and 593.73-keV γ rays, the angular distributions for both γ rays can be separated from that of the composite peak. The values $A_{22} = -0.700 \pm 0.030$, $A_{44} = 0.030 \pm 0.020$ are obtained for the 592.73-keV γ ray and $A_{22} = -0.29(4), A_{44} = 0.00(5)$ for the 592.72-keV γ ray. The DCOQ ratio of the 592.72-keV γ ray was measured to be 1.62 ± 0.22 which implies $\Delta I = -1, \delta \approx 0.0$, completely consistent with the above results. The spin of the 5252.9-keV state must therefore be 13.

If $\delta \approx -0.4$ and $A_{22} = -0.70, A_{44} = 0.03$ are assumed for the $7^+ \rightarrow 6^+$ 592.73-keV γ ray, then $P_{\text{a.d.}} = -0.01$ is predicted (i.e., this γ ray has no polarization). If $\delta \approx 0.0$, and $A_{22} = -0.29$, $A_{44} = 0.00$ are assumed for the $13 \rightarrow 12^+$ 592.72-keV γ ray, then $P_{\text{a.d.}} = -0.38$ is predicted. The linear polarization of the composite 593-keV peak is predicted to be $P_{\text{a.d.}} = -0.17$ or +0.15 for no parity change or parity change, respectively. The measured value $P_{\text{exp}} = -0.10 \pm 0.13$ clearly favors no parity change. Thus the parity of the 5252.9-keV state must be positive.

IV. DISCUSSION

The yrast structure of ^{106}Cd contains features which were also observed in the series ^{102,104,106}Pd (Ref. 4). First, the ground-state band of ^{106}Cd is interrupted above the 6^+ level. That is, the energy spacing in the ground-state band increases monotonically up to the 6^+ level, but the 8^+, 10^+, and 12^+ states clearly do not fit into the same energy sequence. Second, a group of strongly excited negative-parity states also are observed. Above the 8^- and 9^- states, the negative-parity states appear to be members of $\Delta I = 2$ bands which have energy spacing quite similar to the $0^+, 2^+, 4^+, 6^+$ level sequence of the ground-state band. These observations are consistent with a rotational picture in which Coriolis-decoupled bands are based on two-quasiparticle states. (A decoupled band is one in which the $\Delta I = 2$ rotational band of the core appears to be superimposed on a n-quasiparticle bandhead.) In particular, Flaum and Cline[14] have presented the results of two-quasiparticle–plus–rotor calculation for ^{104}Pd. Their results showed convincingly that the analogous break in the ^{104}Pd ground-state band was attributable to the intersection of the zero-quasiparticle band with a decoupled two-quasineutron band of $(h_{11/2})^2$ parentage. The analogous negative-parity bands built on 8^- and 9^- states in ^{104}Pd were attributed to decoupled two-quasiparticle bands of $[h_{11/2}\text{-}g_{7/2}]$ and $[h_{11/2}\text{-}d_{5/2}]$ parentage, respectively. Since ^{106}Cd and ^{104}Pd are isotones, the same results would be expected to apply to ^{106}Cd, with appropriate parameter changes to reflect the change in proton number.

There are, however, several distinctive features of the ^{106}Cd level scheme which have no obvious counterparts in the Pd series. For example, the yrast 8^+ state at 3044.23 keV is far too low in energy to be a member of the zero-quasiparticle band. A similar 8^+ state was observed in ^{108}Cd (Ref. 5) at 3110.54 keV. The yrast 8^+ states in ^{102,104,106}Pd (Ref. 4) are members of the ground-state band. An additional 8^+ state is seen in ^{102,104}Pd several hundred keV above the yrast 8^+ state. Since the energy of these intruder 8^+ states is insensitive to the number of neutrons (essentially the same energies in ^{106,108}Cd), but is sensitive to the proton number (lower energy in Cd than Pd), the states may have large two-quasiproton components. There is other evidence that two-quasiproton configurations are present in low-lying states in Cd isotopes. Auble *et al.*[15] have studied the ^{107,109}Ag(^{3}He, d) ^{108,110}Cd reactions at 27 MeV. Rather strong $l = 4$ stripping strength was observed into the two low-lying 5^- state at 2601 and 2707 keV in ^{108}Cd and 2538 and 2660 keV in ^{110}Cd, the counterparts of the 2629.28- and 2920.21-keV 5^- state in ^{106}Cd. These states must then contain substantial two-quasiproton components.

Because of the similarities, and yet differences, between ^{106}Cd and ^{104}Pd, we have performed a two-quasiparticle Coriolis coupling calculation to interpret the nuclear structure of ^{106}Cd. The calculation is based on the model described in detail by Flaum and Cline[14]; in fact, they were kind enough to furnish a copy of their computer code. A spectrum of states is generated consisting of rotational bands built on two-quasiparticles states. The Coriolis interaction, which has large matrix elements in slightly deformed nuclei, then mixes these basis states. This effect is treated exactly in the calculation. Band mixing through any residual interaction is completely ignored. Flaum and Cline investigated the effects of including a realistic residual interaction, and found that they were small compared to the much larger Coriolis effects. This conclusion is valid as long as states which can be mixed by both interactions are being considered. The Coriolis operator is, however, a single-particle operator, and can only mix two-quasiparticle states which contain a common one-quasiparticle component. Thus admixtures of zero- and two-quasiparticle, or two-quasineutron and two-quasiproton, or two-quasiparticle ($N = 5$) and two-quasiparticle ($N = 4$) states through the Coriolis interaction are not allowed. The appropriate residual interaction could, however, mix any of these

states. Thus one should be wary of results which place states of the same spin and pairity, but from different classes, close together in energy, since the neglect of the residual interaction could result in serious errors.

One modification was made to the calculation. A variable moment-of-inertia treatment is clearly needed to fit energies of ground-state bands in the mass-100 region. Flaum and Cline included this effect only as a scaling factor on the final energies of the calculation. We feel that this approach is inconsistent. The moment of inertia controls the amount of mixing in the calculation, since it scales the Coriolis interaction. Only if the moment of inertia were constant for each basis state of the same total spin I, which it is not, would the inclusion of a variable moment of inertia result in simply scaling the final energies.

We modified the calculation to include explicitly a variable moment of inertia, following a procedure discussed in detail by Smith and Rickey.[1] This procedure is a simple extension to two-quasiparticle bands of the variable moment of inertia (VMI) model.[16] The basic expression for the rotational energy includes an additional potential energy term.

$$E_I = \frac{1}{2\mathcal{I}} [I(I+1) - K^2] + \tfrac{1}{2} C(\mathcal{I} - \mathcal{I}_0)^2 .$$

The variation of the moment of inertia is then governed by the condition

$$\frac{dE}{d\mathcal{I}} I = 0 .$$

The free parameters $\mathcal{I}_0$ and C are restricted by the values required to reproduce the ground-state band of the core. The "moment of inertia" used in off-diagonal matrix elements was an average of those calculated for the two states being mixed. This treatment of the moment of inertia has little effect on the wave functions for high-spin yrast states which are rotation aligned. There is a more marked effect on wave functions of other states, such as the two-quasiproton states from configurations of high K.

There are a reasonably large number of input parameters to the two-quasiparticle calculation which, in the absence of constraints, can be artificially varied to produce misleading results. We have, however, performed extensive one-quasiparticle calculations for odd-A Pd (Ref. 1), Cd (Ref. 2), and Ag (Ref. 17) isotopes, and have used the parameters which successfully described the odd-A nuclei to constrain parameters of the two-quasiparticle calculation. A standard Nilsson[18] calculation was used to obtain single-particle energies and wave functions for the $N=5$ and $N=4$ neutron shells, and for the $N=4$ and $N=3$ proton shells. The shell model parameters κ and μ were selected to give level positions at zero deformation corresponding to those determined for each case by Reehal and Sorenson.[19] These values are listed in Table VI. A deformation of $\delta = 0.12$ was used for all calculations. The position of the Fermi surface is a critical parameter in Coriolis calculations. In principle there should be one neutron and one proton Fermi surface involved. Since, however, the Nilsson calculations for even and odd parity states are independent, there are in practice four parameters involved, one for each shell. For the present calculation the different Fermi surface energies included in Table VI were extracted directly from the separate odd-A calculations. For example, neutron Fermi surfaces were placed halfway between those used for ^{105}Cd and ^{107}Cd. Initial estimates of *VMI* parameters $\mathcal{I}_0$ and C were obtained from fits to the ground-state band up to the 6^+ state. The parameters were then adjusted to give a better overall fit to experimental energies. The parameters listed in Table VI were used for all calculations. Somewhat better fits could have been obtained by varying C for individual bands, but we feel that parameter changes should be kept to a minimum in order to emphasize the physics of the model.

The calculation can, at present, mix only 20 bands, and so the basis must be truncated. The choice of basis states is not straightforward. Since high-spin states are of primary interest in the present work, those bands which contained high-spin states closest to the Fermi surface were included. This in practice means that for two quasineutrons the bands of highest K were neglected, and for two quasiprotons those of lowest K. The Nilsson components utilized are given in Table VI.

A problem exists in discussing final wave functions from the calculation. There are many different components contributing to any of the calculated wave functions, each component consisting of two different Nilsson states coupled to a different value of K. Enumerating the amplitudes of all components becomes cumbersome. Usually there are several Nilsson components with the same shell model parentage. For example, the $\frac{9}{2}+[404]$, $\frac{7}{2}+[413]$, $\frac{5}{2}+[422]$, $\frac{3}{2}+[431]$, and $\frac{1}{2}+[440]$ states all arise, at zero deformation, from the $g_{9/2}$ shell model state. It is convenient to summarize the dominant character of the wave function by giving the shell model parentage of the largest components.

The calculation successfully reproduces many of the features observed in ^{106}Cd. There are of course many states predicted which are too far from the yrast line to have any relation to those observed,

TABLE VI. Parameters used in the calculation. $\delta = 0.12$, $\vartheta_0 = 10$ MeV^{-1}, $C = 0.06$ MeV^3.

N	κ	μ	λ (MeV)	Δ (MeV)	Parity of $2qp$ states	Nilsson orbitals (Single-particle energies in MeV)				Range of $K = \Omega_1 \pm \Omega_2$
5	0.064	0.350	45.90	0.8	+	$\frac{7}{2}-[523]$	$\frac{5}{2}-[532]$	$\frac{3}{2}-[541]$	$\frac{1}{2}-[550]$	0–6
						(48.17)	(47.51)	(47.04)	(46.78)	
					−	$\frac{3}{2}-[541]$	$\frac{1}{2}-[550]$			0–4
						$\frac{5}{2}+[413]$	$\frac{3}{2}+[442]$	$\frac{3}{2}+[411]$	$\frac{1}{2}+[431]$	$\frac{1}{2}+[420]$
4	0.070	0.350	45.0	0.8	+	$\frac{5}{2}+[413]$	$\frac{3}{2}+[442]$	$\frac{3}{2}+[411]$	$\frac{1}{2}+[431]$	$\frac{1}{2}+[420]$ 0–3
						(46.60)	(45.34)	(46.32)	(44.40)	(45.55)
4	0.067	0.435	41.55	1.0	+	$\frac{9}{2}+[404]$	$\frac{7}{2}+[413]$	$\frac{5}{2}+[422]$	$\frac{3}{2}+[431]$	$\frac{1}{2}+[440]$ 2–8
						(42.10)	(41.15)	(40.37)	(39.82)	(39.51)
					−	$\frac{9}{2}+[404]$	$\frac{7}{2}+[413]$	$\frac{5}{2}+[442]$	$\frac{3}{2}+[431]$	2–6
3	0.060	0.435	39.50	1.0		$\frac{3}{2}-[301]$	$\frac{1}{2}-[310]$	$\frac{1}{2}-[301]$		
						(39.34)	(38.16)	(40.55)		

and subsequent discussion will be concerned with the low-lying states of a given spin.

The calculated energies of negative-parity states are compared to those observed experimentally in Fig. 5. The two low-lying 5^- states are predicted to be two-quasiproton states. The wave functions show the two states to be of very different character. The lowest 5^- state is predicted to be predominantly $[g_{9/2}, p_{3/2}]$ coupled to $K = 5$, and the next 5^- state is predicted to be predominantly $[g_{9/2}, p_{1/2}]$ coupled to $K = 5$. The next two 5^- states predicted are two-quasineutron states. The lower is predominantly $[h_{11/2}, d_{5/2}]$ and the higher is predominantly $[h_{11/2}, g_{7/2}]$. These should be too high in energy to be observed, but may mix with the lower-lying two-quasiproton states through the neglected residual interaction. Mixing between two-quasineutron and two-quasiproton states is expected to be more of a factor in the low-lying 6^- and 7^- states. Two of the predicted 7^- states are in fact almost degenerate in energy. Thus the predicted wave functions, and any observables extracted from them such as transition probabilities and branching ratios, may be unreliable. There is, however, reasonable agreement in energies with the 6^- and 7^- states observed experimentally.

At higher spins the predicted two-quasiproton states lie much higher in energy for a given spin than do the two-quasineutron states, thus mixing between these types of states should be small. The

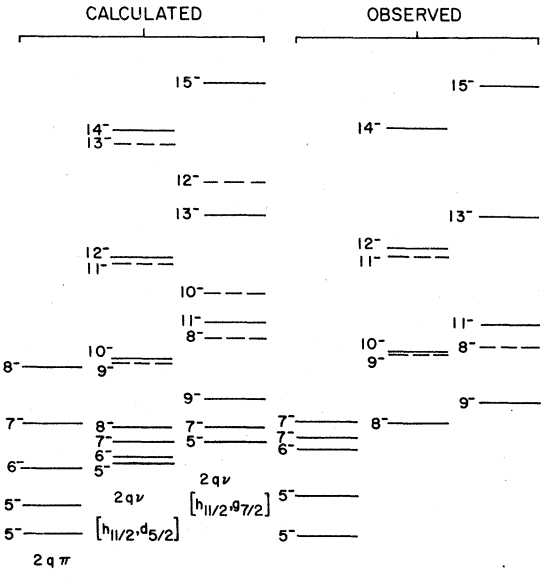

FIG. 5. Comparison of calculated and experimental energy levels for negative-parity states in ^{106}Cd. Dashed levels correspond to nonyrast states discussed in the text.

calculation clearly predicts two bands which are moderately decoupled; one of predominantly $[h_{11/2}, d_{5/2}]$ character, and the other of predominantly $[h_{11/2}, g_{7/2}]$ character. Table VII includes some of the calculated features of these bands. (To facilitate the discussion, subscripts will be used to identify the energy ordering of states of the same spin.) As can be seen in Table VII, the states with the spin sequence 8_1^-, 9_2^-, 10_1^-, 11_2^-, 12_1^-, 13_2^-, and 14_1^-, are all predicted to be of predominantly $[d_{5/2}, h_{11/2}]$ character. The 10^--9^-, 12^--11^-, and 14^--13^- energy spacings are small compared to the 10^--8^-, 12^--10^-, and 14^--12^- energy spacings. Thus because of the energy differences, the yrast cascade would be expected to pick out the even spin states even though the band is not, strictly speaking, decoupled. This prediction agrees with the experimental observation of a relatively intense γ-ray cascade between state of spin 14^-, 12^-, 10^-, and 8^-. States which correspond in both energy and spin to the 9_2^- and 11_2^- states have been observed experimentally. The observed population of these odd spin states is much smaller than that of the corresponding even spin states. The decay of the observed 11_2^- state at 4903.0 keV reinforces its association with the calculated 11_2^- state. The state decays only to other states which appear to be members of the $[d_{5/2}, h_{11/2}]$ band. The states with the spin sequence 9_1^-, 8_2^-, 11_1^-, 10_2^-, 13_1^-, 12_2^-, 15_1^-, and 14_2^- are predicted to be of predominantly $[g_{7/2}, h_{11/2}]$ character. The even spin states have energies substantially higher than those of the odd spin states of the next higher spins. Thus this band is decoupled, and a $\Delta I = 2$ yrast cascade between odd spin states is expected, in agreement with the experimental results. The even spin members of this band would be very hard to populate, and in fact only the 8_2^- state predicted has a possible counterpart in the experimental results.

The main features of the calculation can be understood in terms of the simplified rotation-alignment model.[20] Two simple concepts are presented in this model. The first is that at small deformations Coriolis energies can be large. The energy of a state is lower when the total angular momentum I is aligned with the total quasiparticle angular momentum J, or equivalently when I and the angular momentum of the core R are parallel. States for which this condition is met are described as "rotation aligned", or more commonly just "aligned". The second is that, since rotational energies are large, the aligned state with minimum energy for a given angular momentum is obtained by maximizing the contribution to I from J and

TABLE VII. Summary of calculated negative-parity states.

E (MeV)	I	Fractional composition $[h_{11/2}, d_{5/2}]$	$[h_{11/2}, g_{7/2}]$	$[g_{9/2}, p_{1/2}]$	$[g_{9/2}, p_{3/2}]$	Dominant R
			Two quasineutron			
3.195	5	0.99	0.01	...	...	1.5
3.241	6	0.99	0.01	...	...	2
3.362	5	0.15	0.85	...	...	3
3.373	7	0.60	0.40	...	...	2
3.489	8	0.90	0.10	...	...	2
3.497	7	0.43	0.57			2
3.737	9	0.27	0.73	...	...	2
4.028	9	0.75	0.25	...	...	4
4.054	10	0.99	0.01			2.5
4.215	8	0.36	0.64	...	...	4
4.368	11	0.20	0.80	...	...	3
4.627	10	0.52	0.48	...	...	4
4.838	11	0.81	0.29	...	...	4
4.883	12	0.98	0.02			4.5
5.243	13	0.18	0.82			5
5.554	12	0.46	0.54			6
5.873	13	0.84	0.16			6
5.933	14	0.98	0.02			6
6.327	15	0.16	0.84			6
6.680	14	0.42	0.58			8
7.100	15	0.85	0.15			8
			Two quasiproton			
2.630	5			0.001	0.999	2
2.835	5			0.95	0.05	1
3.537	7			0.83	0.19	4
3.996	8			0.87	0.13	4
4.515	9			0.85	0.1	6

minimizing the contribution from R. In the present context, maximum J is obtained by coupling spins of $d_{5/2}$ and $h_{11/2}$ quasineutrons to $J^\pi = 8^-$, or spins of $g_{7/2}$ and $h_{11/2}$ quasineutrons to $J^\pi = 9^-$. Decoupled bands of aligned states are then obtained with spins $I = J$, $J+2$, $J+4$, etc. and energy spacings similar to those of the core. The states with $I = J+1$, $J+3$, etc., are nonaligned, and lie at higher excitation energies than the aligned states with $I = J+2$, $J+4$, respectively. Good rotation alignment is seen in the higher-spin yrast states of the present calculation. For example, Table VII shows that the yrast 14^- and 15^- state are expected to be $J = 8$, $R = 6$, and $J = 9$, $R = 6$, respectively. At lower spins the alignment is not as good, that is, the most probable value of R for these 8^- and 9^- states is $R = 2$ rather than $R = 0$. Nevertheless, the conceptual roles of the lowest 8^- and 9^- states as bandheads seems firmly established, as evidenced by the regular energy spacings of higher-spin states and the compression in energy of the 7^- and 6^- states.

The overall agreement in energies between the calculation and experiment for negative-parity states as shown in Fig. 5 is excellent. One might ask, however, to what extent this agreement reflects the physics of the model, considering the number of parameters involved. Further insight into the physics of the model can be obtained by investigating the systematics of similar negative-parity states in neighboring Cd and Pd isotopes. Two major effects have been observed experimentally. The first is a decrease in the excitation energies of the 8^- and 9^- bandheads as neutrons are added. For example, between ^{106}Cd and ^{108}Cd (Ref. 5) the 8^- and 9^- bandheads have dropped in energy by 284 and 194 keV, respectively. This same trend was observed in the ^{102,104,106}Pd series. The second effect is that the nonaligned states (i.e., the second 8^-, 9^-, 10^-, 11^-, etc., states) move down in energy relative to the aligned states. This effect is most clearly seen in the comparison of ^{104}Pd and ^{106}Pd (Ref. 4). In ^{108}Pd second 8^- and 9^- bands were, in fact, observed. In the context of the model the addition of two neutrons is simulated to first order by simply increasing the energy of the Fermi surface. Consequently, a calculation was performed in which the only parameter change was an increase in the position of the Fermi surface of 0.5 MeV. (The magnitude of this shift was suggested by the odd-A Pd calculations previously reported.[1]) The comparison of this "^{108}Cd" calculation to the ^{106}Cd calculation and to the pertinent portion of the ^{108}Cd level scheme is shown in Fig. 6. The absolute decreases in energy of the 8^- and 9^- bandheads resulting from this single parameter change agree exceedingly well with the observed decreases. (The calculated energies of higher-spin members of these bands are somewhat compressed relative to the energies observed. It seems that ^{108}Cd is a stiffer rotor than ^{106}Cd. The fit could be improved by an additional change of *VMI* parameters, but this was not done here in order to isolate the role played by the Fermi surface.) The drop in energy of the nonaligned states relative to the aligned states is also predicted. The nonaligned 8^- and 10^- states in fact drop so far that they are the nonaligned states observed in ^{108}Cd, rather than the nonaligned 9^- and 11^- states observed in ^{106}Cd.

The underlying physics responsible for these systematic phenomena is straightforward. All of the Nilsson states of $h_{11/2}$ parentage lie above the Fermi surface in both ^{106}Cd and ^{108}Cd. They are, of course, all closer to the Fermi surface in ^{108}Cd than in ^{106}Cd; hence there is a net decrease in the contribution to the two-quasiparticle energies from $h_{11/2}$ quasiparticles. However, the Fermi surface is moving through the Nilsson states of $d_{5/2}$ and $g_{7/2}$ parentage, and the contribution to two-quasiparticle energies from these quasiparticles remains roughly constant. The decrease in energy of the 8^- and 9^- bandheads is thus due primarily to the drop in energy of the $h_{11/2}$ quasiparticles. An interesting parallel exists between these 8^- and 9^- bandhead energies in ^{106}Cd and ^{108}Cd, and the energies of the lowest $\frac{5}{2}^+$, $\frac{7}{2}^+$, and $\frac{11}{2}^-$ states in ^{105}Cd and ^{107}Cd.[2] The ground state of both ^{105}Cd and ^{107}Cd is a $\frac{5}{2}^+$ state. The energy of the $\frac{11}{2}^-$ state drops from 1163 keV in ^{105}Cd to 846 keV in ^{107}Cd, while the $\frac{7}{2}^+$ energy rises from 131 keV in ^{105}Cd to 205 keV in ^{107}Cd. One can simply compare summed one-quasiparticle energies in ^{105}Cd to summed energies in ^{107}Cd in order to estimate energy shifts for the 8^- and 9^- state in ^{106}Cd and ^{108}Cd. The estimated decreases

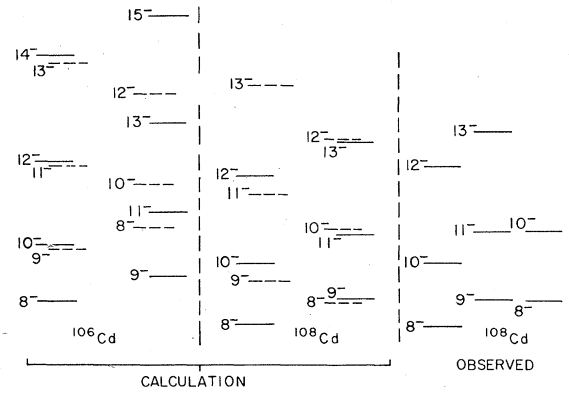

FIG. 6. Systematic shifts calculated for the 8^- and 9^- bands between ^{106}Cd and ^{108}Cd, compared to levels observed in ^{108}Cd: The only change in the calculation was a shift of the Fermi surface. Dashed levels correspond to nonyrast states.

in energy are 317- and 243-keV compared to observed decreases of 284- and 194-keV for the 8^- and 9^- bandheads, respectively. The dominant contribution is from the large change in energy of the $\frac{11}{2}^-$ state, with a minor effect due to the small change in energy of the $\frac{7}{2}^+$ state.

While the rise of the Fermi surface through the Nilsson states of $d_{5/2}$ and $g_{7/2}$ parentage has little effect on the bandhead energies, it has a large effect on the nonaligned states. The Fermi surface is moving from low to high values of Ω for the $d_{5/2}$ and $g_{7/2}$ Nilsson states. Thus the extent of decoupling in bands involving these components decreases, and the nonaligned states move down in energy relative to the aligned states. This trend toward strong coupling as the neutron number increases is seen both in the calculation and the experimental results. Again a strong parallel with odd-A nuclei in the region can be found. Bands built on $\frac{11}{2}^-$, $\frac{7}{2}^+$ and $\frac{5}{2}^+$ states have been observed in a number of Cd[2] and Pd[1] nuclei. In ^{101}Pd all three bands are decoupled. As neutrons are added to obtain ^{105}Pd, the $\frac{11}{2}^-$ band remains decoupled and the $\frac{7}{2}^+$ band becomes marginally decoupled, while the $\frac{5}{2}^+$ band becomes strong-coupled.

Calculations for positive-parity states were also performed. The results are, however, more difficult to interpret than those for negative-parity states because of the neglected residual interactions. Figure 7 shows a comparison of calculated energy levels to those observed. The figure contains four classes of calculated states, all of which are noninteracting in the framework of the model. The first is a band of zero-quasiparticle states where energies are obtained by a simple *VMI* fit to the 0^+, 2^+, 4^+, and 6^+ members of the ground-state band. The second is a group of two-quasineutron states resulting from the various couplings of Nilsson states of $d_{5/2}$ and $g_{7/2}$ parentage. The third are two-quasineutron states of $h_{11/2}$ parentage. The last are two-quasiproton states due to the coupling of states with $g_{9/2}$ parentage. In several instances, states of the same spin from different classes are predicted to have almost the same energy. Thus the states must mix to some extent, and a detailed comparison of the calculation and the experimental decay scheme is probably pointless. In spite of this difficulty, however, the calculation sheds some light on many of the features observed.

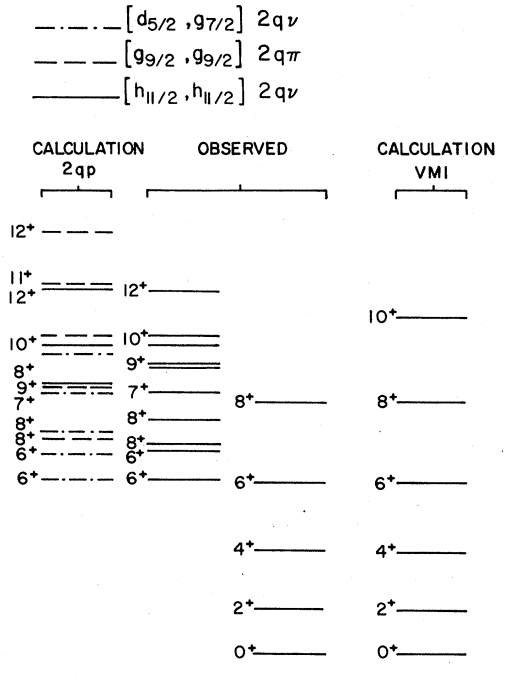

FIG. 7. Comparison of calculated and experimental energy levels for positive-parity states in ^{106}Cd.

The low-lying 6^+ and 7^+ states (2503.14, 2924.93, and 3127.27 keV, respectively) are identifiable with two-quasineutron states from the $[d_{5/2}, g_{7/2}]$ basis. There is probably some mixing between the 2503.14-keV 6^+ state and the 6^+ member of the ground band. The calculation predicts that the dominant R components for the lowest 6^+ state are $R=2$ and 4, thus this mixing may be inhibited due to the small overlap of the $R=6$ components.

Three 8^+ states are observed experimentally. The lowest 8^+ state (3044.23 keV) corresponds nicely in energy to a two-quasiproton state, predicted to be predominantly a $K=8$ state from the coupling of $g_{9/2}$ Nilsson quasiprotons. The model clearly predicts that a $K=8$ two-quasiproton band should lie at a lower excitation energy in Cd isotopes than in Pd isotopes. Again, this is a result of the shift in the proton Fermi energy towards higher values of Ω in Cd nuclei. If the proton Fermi surface is moved downward by 500-keV to simulate ^{104}Pd, the predicted excitation energy of the 8^+ bandhead moves up by some 400-keV. This would place the 8^+ two-quasiproton state above the 8^+ member of the ground band, and corresponding states have in fact been observed in ^{102}Pd and ^{104}Pd. A $\Delta I=1$ band built on the low-lying 8^+ state in ^{106}Cd is predicted. Because this band is strong-coupled, the rotational spacings should be large, and higher members of the band should lie above the yrast line. The 9^+ and 10^+ member of this band may be the 4121.02- and 4574.4-keV states observed experimentally. A second 8^+ state from the $[d_{5/2}, g_{7/2}]$ basis is predicted at a somewhat higher excitation energy than the 8^+ two-quasiproton state. This state may correspond to the 8^+ 3367.29-keV state. The zero-quasiparticle 8^+ state is predicted by the *VMI* model to lie at a still higher energy, and agrees in energy with the 8^+

3641.7-keV state. The model predicts that a fourth 8^+ two-quasiparticle state from the $h_{11/2}$ basis lies still higher in energy. The dilemma that one must face is that all four 8^+ states predicted lie close enough in energy that mixing must occur, thus all of the comparison with experiment must be taken with reservation.

Finally, a 10^+ decoupled band is predicted. This band, with origin in the $h_{11/2}$ basis, has been claimed to be responsible for backbending in neighboring Cd and Pd nuclei, where members of such a band may be identified up to high spins (18^+ in ^{104}Pd). The investigation of these backbending phenomena were in fact the impetus for developing the initial two-quasiparticle calculations. In ^{106}Cd, however, this band seems to play a minor role. The 10^+ and 12^+ states observed at 4436.08 and 5241.06 keV do correspond to predicted members of this band. The nature of the bandhead itself is questionable. The calculation predicts three 10^+ states which are almost degenerate in energy; thus the observed state at 4436.08 keV may be considerably mixed, as its decay suggests. Higher-spin members were not observed, because of the yrast cascade feeding the 12^+ state at 4659.81 keV.

This abnormally low-lying 12^+ state is a fascinating feature of ^{106}Cd. It appears to be the bandhead for a $\Delta I = 1$ band which has no counterpart in the two-quasiparticle calculation. Daniere *et al.*[6] have measured the half life of this state to be 62 ± 6 ns. The 223.61-keV $E2$ transition from this level is therefore retarded by a factor of 3.7 over the Weisskopf single-particle estimate and the 335.34-keV $E1$ transition is retarded by a factor of 1.68×10^7. Daniere *et al.*[6] suggests that this state has a four-quasiparticle configuration $[\pi(g_{9/2})^{-2}8^+\nu(d_{5/2})^2 4^+]12^+$.

V. CONCLUSIONS

The previously proposed level scheme for ^{106}Cd based on the results of $(\alpha, 2n\gamma)$ reaction[6] has been greatly expanded in the present work, with many new high-spin states (up to spin 15 and excitation energy 6265 keV) populated by (heavy-ion, $xn\gamma$) reactions. Many features of ^{106}Cd are similar to those of ^{108}Cd (Ref. 5) and ^{102,104,106}Pd (Ref. 4), consisting of collective structure based on the ground and excited states. The proposed level scheme is in excellent agreement with the results of a calculation which treats ^{106}Cd as a slightly deformed rotor. In this model the excited states of ^{106}Cd are represented by rotational bands built on two-quasiparticle states, which are mixed by the Coriolis interaction. The calculation shows convincingly that the yrast 10^+, 9^-, and 8^- bands can be interpreted as two-quasineutron states with rotational bands built on them. The calculation also shows that two-quasiproton states play an important role in ^{106}Cd. The energies of the yrast 8^+ state and a band built on it, and also the energies of the lowest 5^- state agree well with those predicted from the two-quasiproton calculation. The basic systematic behavior of all these features in neighboring even-even nuclei has been seen to be consistent with the rotational model, with only the position of the Fermi surface varied. In fact, the only high-spin states observed which do not have reasonable counterparts in the calculation are populated in the cascade feeding the 4659.81-keV 12^+ state; it has been suggested that this band has four-quasiparticle parentage.[6]

The ^{106}Cd level scheme proposed here and the successful description of it by a rotational model present additional evidence that mass-100 nuclei are slightly deformed rotors. The basic model used, which has also been successfully applied to neighboring odd-A nuclei, differs from the rotational model widely accepted for the interpretation of strongly deformed nuclei only in the inclusion of a variable moment of inertia. It is clear, however, that the issue is not settled. The energy level predictions for high-spin states observed in (HI, $xn\gamma$) reactions are good. There are other observables, such as transition probabilities and branching ratios, for which no model interpretations have been attempted as yet. There are also lower-spin states observed in the present work (and in other investigations) which have not been treated. Perhaps other degrees of freedom must be considered to successfully describe this more complete set of data. It is, however, by no means impractical to extend the range of the present calculation. Electromagnetic matrix elements can be calculated in a straightforward manner, and many low-spin predictions (not discussed here) are available from the calculation. It was felt that in order to attempt model comparisons in these areas the residual interactions must be treated realistically. Motivated by the success of the present calculations, we are planning further work in this direction, in the hope that a more complete understanding of the structure of transitional nuclei is at hand.

This work was supported by the National Science Foundation.

*Present address: Nuclear Physics Laboratory, University of Colorado, Boulder, Colorado 80304.
†Present address: Schlumberger-Doll Research Center, P. O. Box 307, Ridgefield, Connecticut 06877.

[1]Hastings A. Smith, Jr. and F. A. Rickey, Phys. Rev. C 14, 1946 (1976).
[2]L. E. Samuelson, J. A. Grau, F. A. Rickey, and P. C. Simms (unpublished).
[3]J. W. Starner and M. E. Bunker (private communication).
[4]J. A. Grau, L. E. Samuelson, F. A. Rickey, P. C. Simms, and G. J. Smith, Phys. Rev. C 14, 2297 (1976).
[5]L. E. Samuelson, F. A. Rickey, J. A. Grau, S. I. Popik, and P. C. Simms, Nucl. Phys. A301, 159 (1978).
[6]J. Daniere, R. Beraud, M. Meyer, R. Roughny, J. Genevey-Rivier, and J. Treherne, Z. Phys. A280, 363 (1977).
[7]P. C. Simms, G. J. Smith, F. A. Rickey, J. A. Grau, J. R. Tesmer, and R. M. Steffen, Phys. Rev. C 9, 684 (1974).
[8]D. C. Stromswold, D. O. Elliot, Y. K. Lee, L. E. Samuelson, J. A. Grau, F. A. Rickey, and P. C. Simms, Phys. Rev. C 17, 143 (1978).
[9]K. S. Krane, R. M. Steffen, and R. M. Wheeler, Nucl. Data A11, 351 (1973).
[10]J. A. Grau, F. A. Rickey, G. J. Smith, P. C. Simms, and J. R. Tesmer, Nucl. Phys. A229, 346 (1974).
[11]V. Metag, R. Repnow, and J. L. Durrell, Phys. Lett. 38B, 19 (1972).
[12]S. Flanagan, R. Chapman, J. L. Durell, W. Gelletly, and J. N. Mo, J. Phys. G 2, 589 (1976).
[13]T. Yamazaki, Nucl. Data A3 (No. 1), 1 (1967).
[14]C. Flaum and D. Cline, Phys. Rev. C 14, 1224 (1976).
[15]R. L. Auble, D. I. Horen, F. E. Bertrand, and J. B. Ball, Phys. Rev. C 6, 2223 (1972).
[16]M. A. J. Mariscotti, G. Scharff-Goldhaber, and B. Buck, Phys. Rev. 178, 1864 (1969).
[17]R. K. Popli, J. A. Grau, S. I. Popik, F. A. Rickey, L. E. Samuelson, and P. C. Simms (unpublished).
[18]S. C. Nilsson, K. Dan. Vidensk. Selsk. Mat.-Fys. Medd. 29, No. 16 (1955).
[19]B. Reehal and R. Sorenson, Phys. Rev. C 2, 819 (1970).
[20]F. S. Stephens, R. M. Diamond, and S. G. Nilsson, Phys. Lett. 44B, 429 (1973).